VŠB TECHNICKÁ UNIVERZITA OSTRAVA | FAKULTA ELEKTROTECHNIKY A INFORMATIKY

CENTRUM DOPRAVNÍHO VÝZKUMU

AVISON (Analýza viditelnosti účastníků silničního provozu za účelem zvýšení jejich bezpečnosti za soumraku a v noci)

*je projektem soutěže VI - Bezpečnostní výzkum České republiky 2015-2022 (2015 - 2022) vyhlášeného MV0 - Ministerstvem vnitra (MV) s identifikačním číslem **VI20172019071** řešeným v období: 01.01.2017- 31.12.2019. Jeho hlavní příjemcem je Vysoká škola báňská - Technická univerzita Ostrava / Fakulta elektrotechniky a informatiky, dalším účastníkem projektu je Centrum dopravního výzkumu, v. v. i. v roli dalšího účastníka projektu.*

MINISTERSTVO VNITRA ČESKÉ REPUBLIKY

V Příloze č. 1 Smlouvy – Projekt, v části 5. 3. Vedlejší výsledky projektu:

DEFINICE DRUHŮ VÝSLEDKŮ

(Metodiky hodnocení výzkumných organizací a programů účelové podpory výzkumu, vývoje a inovací schválené usnesením vlády dne 8. února 2017 č. 107)

J_{SC} - recenzovaný odborný článek

Obsah:

1) STRATIL, T., KOUDELKA, P., MARTINEK, R. a NOVAK, T. Active Pre-Equalizer for Broadband over Visible Light. Advances in Electrical and Electronic Engineering, 15(3), (2017), pp. 553 - 560. DOI:10.15598/aeee.v15i3.2210.
2) LATAL, J., KRALIK, M., WILCEK, Z., KOLAR, J. a J. VOJTECH Deployment and Measurement of Quality of Service Parameters for Triple Play Services in Optical Access Networks. Komunikácie, 19(3), (2017). ISSN 2585-7878.
3) VITASEK, J. LATAL, J., STRATIL, T., HEJDUK, S., VANDERKA, A., HAJEK, L. a R. MARTINEK. Purposeful Suppression and Reconstruction of White Light from LED for Improvement of Communication Properties. Advances in Electrical and Electronic Engineering. 17(1), (2019), pp. 74 – 80. DOI: 10.15598/aeee.v17i1.2671
4) LATAL, J., P. HANULAK, J. KOLAR, Z. WILCEK, T. STRATIL AND F. SARLEJ. Measurement of Colour Coordinates of LEDs Used in the Automotive Exterior Lighting. International Journal of Electrical and Computer Engineering (IJECE) Q2, (přijato k publikování). 2020. ISSN 2088-8708.

Active Pre-Equalizer for Broadband over Visible Light

Tomas STRATIL[1], *Petr KOUDELKA*[1], *Radek MARTINEK*[2], *Tomas NOVAK*[3]

[1]Department of Telecommunications, Faculty of Electrical Engineering and Computer Science, VSB–Technical University of Ostrava, 17. listopadu 15, 708 33 Ostrava, Czech Republic
[2]Department of Cybernetics and Biomedical Engineering, Faculty of Electrical Engineering and Computer Science, VSB–Technical University of Ostrava, 17. listopadu 15, 708 33 Ostrava, Czech Republic
[3]Department of General Electrical Engineering, Faculty of Electrical Engineering and Computer Science, VSB–Technical University of Ostrava, 17. listopadu 15, 708 33 Ostrava, Czech Republic

tomas.stratil@vsb.cz, petr.koudelka@vsb.cz, radek.martinek@vsb.cz, tomas.novak1@vsb.cz

DOI: 10.15598/aeee.v15i3.2210

Abstract. *This paper introduces a new technology called Broadband over Visible Light (BVL) which combines two technology solutions like Visible Light Communication(VLC) and Broadband over Power Line (BPL). This new technology is suitable for converting modern LED lighting systems into communication systems. However, there are some deficiencies in BVL technology such as the low bandwidth of LED optical transmitters. Pre-equalization may be solution of this problem. This paper proposes higher bandwidth using the pre-equalization circuit. Also, it shows real experimental results demonstrating an improvement of bandwidth and transmission rate.*

Keywords

Equalization, Labview, pre-equalizaton, Software-defined radio, Visible Light Communication, VLC.

1. Introduction

The recent development in the area of white LEDs caused their common use as a highly efficient alternative to the conventional sources of optical radiation in the visible range. This development brought progressive changes in the lighting technology. The physical principle of white LEDs allows their use for communication purposes. The physical principles, including changes in trends of the lighting technology, caused the emergence of a new research direction generally called Visible Light Communication (VLC), which is a derivative of original research direction generally known as indoor Optical Wireless Communication (indoor OWC), operating exclusively in the infra-red spectrum of optical radiation. The objective of this research direction is merging lighting and communications [1], [2] and [**?**].

The Broadband over Visible Light (BVL) is a new research direction based essentially on VLC technology. Again, it is intended to utilize the visible spectrum of optical radiation as a communication direction to the end user (downlink) and to utilize the infra-red spectrum of optical radiation (940 nm) in the reverse communication direction (uplink). Moreover, compared to the VLC concept, in the case of BVL, it is intended to use the chipset of the Broadband over Power Line (BPL) technology, which, inter alia, allows the use of the OFDM MQAM modulation format at the number of 1155 sub-carriers in the frequency range from 2 MHz to 32 MHz (for example HomePlug AV). The BVL technology should, by its nature, enable transmission speed of 100 Mb·s^{-1}. Additionally, the BVL technology provides connectivity over power conductors in an efficient way. It gives us the opportunity to transmit the modulated signal to the optical transmitter by its power lines, and use visible light as a wireless data transmitter.

White light LEDs as transmitters for communication link have the big disadvantage as low bandwidth. Low bandwidth is caused by optoelectronic response of the LED and due to physical principles of fluorescence in a thin layer of phosphor which is responsible for creating white light from blue light. Fluorescence inserts some delay to the optical signal and thus influences the maximum bit rate. White power LEDs achieve several MHz of bandwidth [8]. Some researchers achieve

10 MHz of bandwidth due to optical band pass filter on detection side, where only blue part of wavelength processes pass on photodetector without delayed yellow part from fluorescence. Equalization techniques are used for elimination of LEDs optoelectronic response to achieve higher bandwidth [6] and [7]. This article deals with this actual issue and brings new unpublished results, which can help to develop BVL technology.

2. Bandwidth of LEDs

Broadband Power Line technology operates in the frequency range from 2 MHz to 32 MHz at HomePlug AV specification and provides a 200 Mb·s^{-1} PHY channel rate and 150 Mb·s^{-1} information rate. Suitable bandwidth of optical transmitter has to be reached for cooperating HomePlug AV specification with VLC. The frequency response of high power light LED Philips Fortimo LED DLM 3000 44 W/830 was measured. Network analyzer Rhode-Schwarz ZVB 4 (3 kHz to 4 GHz) [9] was used with our own designed circuit Bias-T [12]. PIN photodetector Thorlabs PDA10A-EC was applied on detection side. Philips Fortimo LED DLM 3000 44 W/830 has system efficiency 62 lm/W. This LED light source offers an advantage for VLC measuring and testing, because of its concept of construction. There were used blue LED chips, which are directly placed on the aluminum block for effective cooling. External diffuser in front of blue LED chips converts part of blue (lower) wavelengths range into higher wavelengths due to phosphor layer as seen in Fig. 1. This white light LED has patented remote phosphor technology. This LED light source meets requirements for future duplex communication. Photodetector operating in the infrared wavelength range could be used behind diffuser with the phosphor layer. Measured values of frequency response were fitted by cubic function to eliminate roughness caused by noise and other signal distortion. The smoother curve of frequency response provides ideal conditions to design the pre-equalization circuit. −3 dBm bandwidth was achieved at 2 MHz with a high power white light LED as shown in Fig. 6, and at 7 MHz with blue part of radiation without phosphor effect.

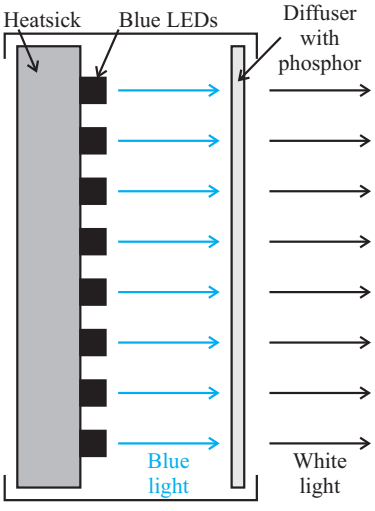

Fig. 1: Concept of Philips FORTIMO LED DLM 3000.

2.1. Design of Pre-Equalizer

The purpose of equalization is to compensate signal distortion in a communication channel. The main distortion of the signal was produced by the optical transmitter at VLC channel due to an optoelectronic response of LED and delay of the phosphor [6]. We used well-known equalization techniques and techniques for designing filters to reach suitable bandwidth. Appropriate bandwidth was reached with a really simple electronic circuit, because the simplicity of designed circuit was the important requirement.

Pre-equalization circuit was designed according to the reversal of measured frequency response, which can be seen in Fig. 6. The circuit is composed of an active and mainly passive part, which determines shape of frequency response. The passive part of the circuit is high pass filter, which causes 35 dBm attenuation, as it can be seen in Fig. 3. The active part of the circuit contains operational amplifier OPA847 eliminating attenuation of the passive part. The complete circuit provides frequency response closed to the reversal of measured frequency response. Circuit diagram of pre-equalizer can be seen in Fig. 2. The transfer function of the pre-equalization circuit was expressed as:

$$H(j\omega) = \left(1 + \frac{R_5}{R_4}\right) \cdot \frac{R_3}{\dfrac{R_2}{j\omega R_2 C + 1} + R_3}, \qquad (1)$$

where ω is defined as $2\pi f$.

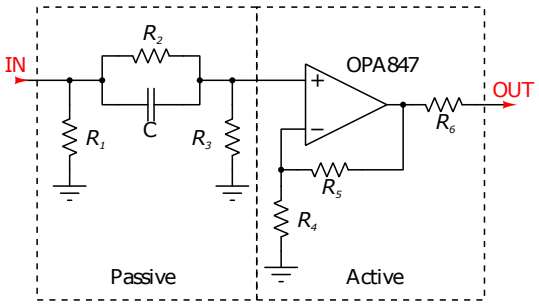

Fig. 2: Circuit diagram of active pre-equalizer with OPA847.

2.2. Simulations

Passive part of the circuit shapes the curve of frequency response and contains parallel connection of resistor R_2

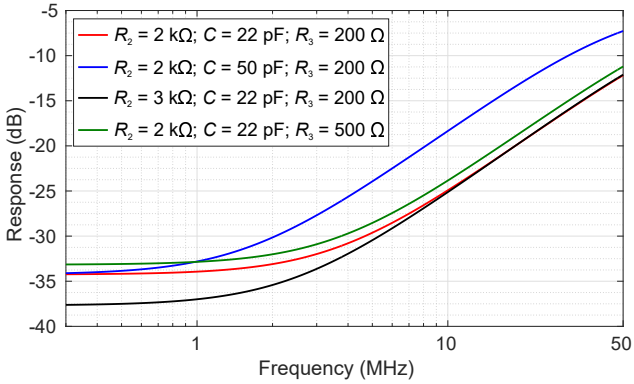

Fig. 3: Simulation results of pasive part of pre-equalizer and effect components values on frequency response.

and capacitor C and resistor R_3, parallelly connected to them. Figure 3 shows the curves from simulations, where the effect of components values on the shape of frequency response can be noticed. The best result of reversal frequency response was reached by the components $R_2 = 2$ kΩ, $C = 22$ pF and $R_3 = 200$ Ω.

Operational amplifier OPA847 was used in active part of the pre-equalization circuit. The OPA847 provides a unique combination of a very low input voltage noise, along with a very low distortion output stage to give one of the highest dynamic range of op amps available. Voltage-feedback of op amps, unlike current-feedback designs, can use a wide range of resistor's values to set up their gain. R_4 was set to 39.2 Ω and R_5 was optimized according to desired gain. Using this guideline ensures that the noise added at the output due to the Johnson noise of the resistors does not significantly increase the total noise over the 0.85 V/$\sqrt{\text{Hz}}$ input voltage noise for the op amp itself. This R_4 value is suggested as a good starting point for the design of the circuit.

Curves gained by simulations of different adjusted values of feedback resistor R_5 are shown in Fig. 4,

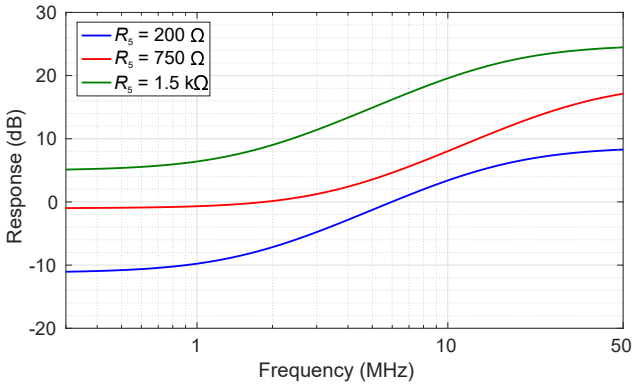

Fig. 4: Simulation results of active part of pre-equaliser and different feedback resistor values effect on frequency response.

where open-source simulation software Qucs was used. R_4 value was 39.2 Ω whereas we were trying to achieve ideal amplification for the pre-equalization circuit by adjusting value R_5. $R_5 = 750$ Ω provided the best result of reversal frequency response and achieved gain +20 V/V of operation amplifier. Values of R_4 and R_5 affected complete amplification of active part of the circuit. On the other hand, they also affected shape of the frequency response of overall pre-equalization circuit as shown in Fig. 4.

2.3. Measurement

The frequency response of constructed pre-equalizer was measured and the results were compared with simulations. Network analyzer Rhode-Schwarz ZVB 4 (3 kHz to 4 GHz) was used. Results from simulations, measurements and reverse are shown in the Fig. 5. Frequency response from simulations and measurements of the pre-equalization circuit are almost same to the reverse frequency response, which is desirable. Operational amplifier OPA847 operates up to 40 MHz as seen in Fig. 5. This is due to high amplification of OPA847, however 40 MHz is sufficient for BVL technology solution. The designed pre-equalizer circuit attenuates the input signal by about 1 dBm in the frequency range 0.2 to 2 MHz. Designed and constructed circuit achieves power level 15 dBm at 40 MHz. Bandwidth from 2 MHz to 40 MHz of designed circuit is compliant according to HomePlug AV technology solution of Broadband Power Line communication.

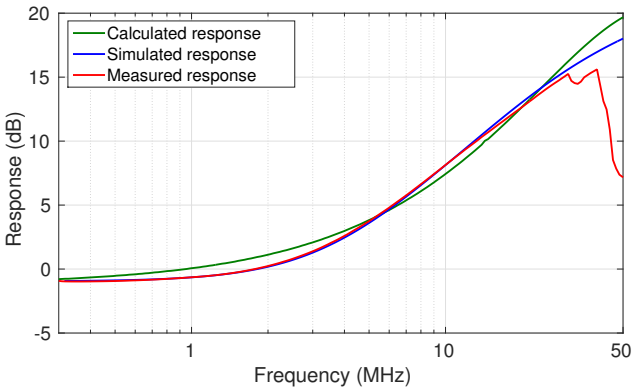

Fig. 5: Frequency response of designed circuit given by reverse, simulation and measurement.

3. Testing Effect of Pre-Equalizer on Bandwith and Modulation

To verify designed and constructed pre-equalizer effect, a new measurement was done on Philips Fortimo LED

DLM 3000 44 W/830 by aforementioned vector network analyzer. The frequency response of LED light source without designed circuit was measured at first, then with pre-equalizer. To allow determining influence of fluorescence in the phosphor, measurement was repeated without diffuser with the phosphor layer on the mentioned white light LED source. Uniform distance 40 cm between the optical transmitter and photodetector was set.

The pre-equalizer measurement results are shown in Fig. 6. It is evident how designed circuit of pre-equalizer influences frequency response of phosphor based white light and also blue part of radiation without influencing the delay due to fluorescence at phosphor layer. A bandwidth of −3 dBm was achieved at 2 MHz with white light LED without pre-equalization, whilst, a bandwidth of −10 dBm was achieved at 6 MHz. In the case of white light LED without pre-equalization, −3 dBm bandwidth was achieved at 2 MHz and −10 dBm bandwidth at 6 MHz. When with the pre-equalization circuit connected between the network analyzer and Bias-T, −3 dBm bandwidth was obtained at 3 MHz and −10 dBm bandwidth at 40 MHz. It proves how pre-equalization mitigates natural inclinations to low bandwidth of semiconductor phosphor based LED light transmitters. The bandwidth of blue part of radiation without the effect of luminescence achieved amplification by 5 dBm at 20 MHz frequency due to pre-equalization.

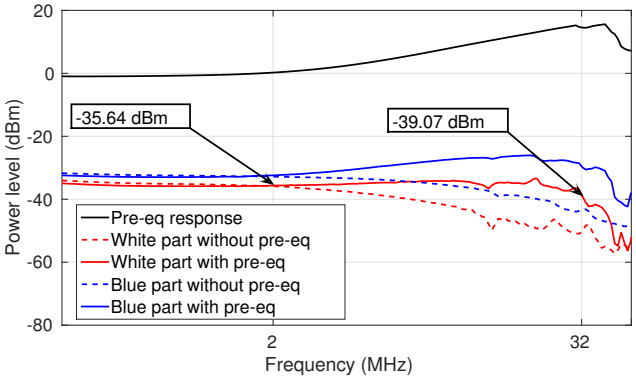

Fig. 6: Effect pre-equalizer on frequency response of white light LED and blue light LED.

The power level of the signal has higher inclination to drop toward increasing frequency, due to influence of phosphor layer. Diffuser with phosphor layer decrease power level. BVL technology with respect to HomePlug AV technology solution operates from 2 MHz to 32 MHz, hence BVL solution needs to achieve this bandwidth. An attenuation of 3.43 dBm was achieved with mentioned bandwidth due to designed pre-equalization circuit.

3.1. Experimental Setup

The block diagram for the experimental setup is shown in Fig. 7. RF VSG NI PXI-5670 (Vector signal generator) [11] was used to generate the digitally modulated signal. MQAM digital modulation was tested [10] and [14], 4QAM was used specifically.

Vector signal analyzer RF VSA NI PXI-5661 [11] was used on the receiver side. The signal modulated by a digital modulation scheme was monitored by constellation diagram and simultaneously an Error Vector Magnitude (EVM) was measured. The EVM provides a comprehensive measure of the quality of the digitally modulated signal. We used it to verify pre-equalization circuit effect on the transmitted digital signal, depending on the symbol rate (used bandwidth).

SI PIN photodetector ThorLabs PDA10A-EC is operating in the wavelength range from 200 nm to 1100 nm. Photodetector PDA10A-EC has an effective area $A_{eff} = 0.8$ mm^2 only, therefore N-BK7 Plano-Convex Lens with a focal length of 25.4 mm was used. Thanks to the lens, an adequate signal output was obtained to verify the functionality at a realistic distance of 3 m between transmitter and receiver. Center frequencies 5 MHz, 10 MHz, 15 MHz and 20 MHz were used in digital modulation scheme.

The detected signal can be represented by:

$$y(n) = g(n)x(n) + \eta(n), \tag{2}$$

where $g(n)$ and $\eta(n)$ represent the multiplicative and additive impairments to the detected signal. The multiplicative impairments can be a result of channel estimation errors or IQ imbalances, for example. The additive impairments are usually caused by thermal noise and are modeled as an *i.i.d.* (Independent and Identically Distributed random variables) complex AWGN samples with Power Spectral Density (PSD) of $N_0/2$.

EVM can be designed as the root-square (RMS) value of the difference between an array of measured symbols and ideal symbols. The EVM can be represented as:

$$EVM_{RMS} = \sqrt{\frac{\frac{1}{N}\sum_{n=1}^{N}|S_r(n) - S_t(n)|^2}{P_0}}, \tag{3}$$

where N is the number of symbols over which the value of EVM is measured. $S_r(n)$ is the normalized received n^{th} symbol which is disrupted by Gaussian noise. $S_t(n)$ is the ideal transmitted value of the n^{th} symbol $x(n)$, and P_0 is either the maximum normalized ideal symbol power or the average power of all symbols for the

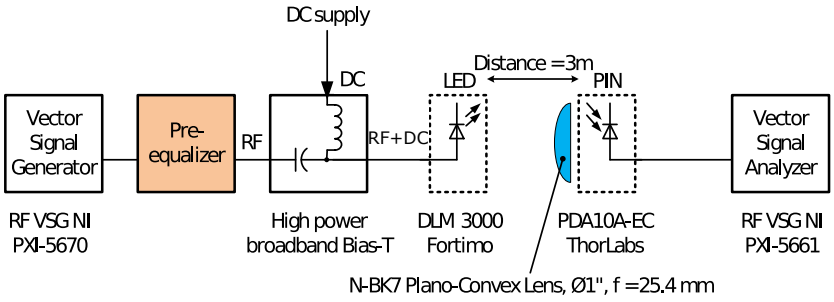

Fig. 7: Block diagram of experimental measurement.

chosen modulation. P_0 can be represented by:

$$P_0 = \frac{1}{M}\sum_{m=1}^{M}|S_m|^2. \tag{4}$$

The EVM value is normalized with average symbol energy to remove the dependency of EVM on the modulation order. Consider the detected signal in Eq. (2), where $g(n) \approx 1$. For non-data-aided receivers, the EVM is:

$$EVM_{RMS} = \sqrt{\frac{\frac{1}{N}\sum\limits_{n=1}^{N}|y(n)-\tilde{x}(n)|^2}{P_0}}, \tag{5}$$

where $\tilde{x}(n)$ are transmitted symbols, which are estimated and used to measure the EVM value.

According to [13], the EVM for QAM signals is:

$$\begin{aligned} EVM_{QAM} &= \\ &= \left[\frac{1}{SNR} - 8\sqrt{\frac{3}{2\pi(M-1)SNR}}\sum_{i=1}^{\sqrt{M}-1}\gamma_i e^{\frac{3\beta_i^2 SNR}{2(M-1)}}\right. \\ &\left. + \frac{12}{M-1}\sum_{i=1}^{\sqrt{M}-1}\gamma_i\beta_i \mathrm{erfc}\left(\sqrt{\frac{3\beta_i^2 SNR}{2(M-1)}}\right)\right]^{1/2}, \end{aligned} \tag{6}$$

where

$$\gamma_i = 1 - \frac{i}{\sqrt{M}}, \text{ and } \beta_i = 2i - 1. \tag{7}$$

The EVM of a QAM signal in Eq. (6) can be divided into two parts. The first part is 1/SNR, which represents the ideal EVM when no errors are introduced to the symbol detection. The second part is QAM signal, which is the sum of the exponential and error function, representing the reduction in measured EVM due to the error detection.

3.2. Results and Discussions

The results were measured by the block diagram shown in Fig. 7. 4QAM digital modulation scheme was transmitted via white part of radiation with effect of the luminescence and results are shown in Fig. 8. Small differences were measured between EVM values of VLC system without the pre-equalizaion circuit and with pre-equalization for center frequency 5 MHz. The pre-equalization circuit had significant influence at higher frequencies.

Significant improvement of EVM values was verified with VLC system with pre-equalization. Most significant difference of EVM values was for center frequency of 20 MHz due to frequency response of pre-equalization circuit seen in Fig. 6. EVM value increased when symbol rate was increased, due to non-linearity of frequency spectrum.

EVM values were increased due to low signal power level and natural inclinations of the frequency response as shown in Fig. 6. Higher bandwidth was used with higher symbol rate and it increased EVM and decreased communication possibility because of inadequate frequency response. The VLC system was not suitable for use in higher central frequencies and higher bandwidth for digital modulations without pre-equalization. The VLC system with the pre-equalization circuit provided compliant conditions, thus higher central frequencies and bandwidth could be used.

4. Conclusion

In this paper pre-equalization of VLC transmitter has been presented. In order to get suitable frequency response of VLC transmitter based on phosphor white LED light source, we have been proposed equalization circuit used in our VLC system. The aforementioned HomePlug AV technology bandwidth from 2 MHz to 32 MHz was achieved with 3.43 dBm attenuation by commercial phosphorescent white light LED and proposed equalizer circuit. The objectives of this paper were to achieve suitable frequency response for the mentioned BVL technology solution. The proposed system demonstrably improves operational bandwidth in VLC system and could be considered as suitable system improvement for future Broadband over Visible Light (BVL) technology deploy.

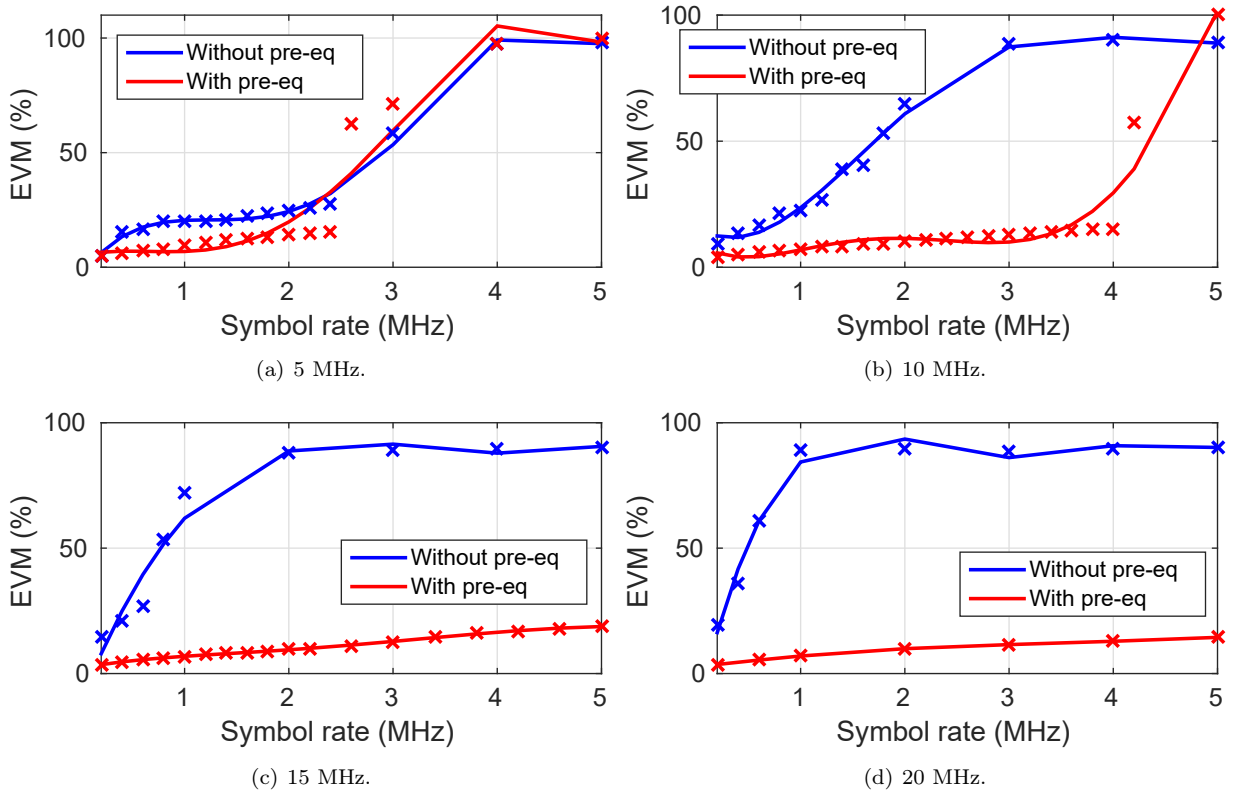

(a) 5 MHz. (b) 10 MHz.

(c) 15 MHz. (d) 20 MHz.

Fig. 8: Resulst of measurement EVM depending on symbol rate and carry frequency transmit 4QAM modulation via white light LED.

Acknowledgment

The research described in this article could be carried out thanks to the active support of the Ministry of Education of the Czech Republic within the projects no. SP2017/97: Remote Control of Public Lighting Luminaires via the Smart Technology Support and SP2017/128: Virtual instrumentation for the measurement and testing IV. This article was supported by projects Technology Agency of the Czech Republic TG01010137: BroadbandLIGHT. The research has been partially supported by the Ministry of Interior of the Czech Republic through grant project MVCR No. VI20172019071: Analysis of visibility of transport infrastructure for safety increasing during night, sunrise and sunset.

References

[1] MCCULLAGH, M. J. and D. R. WISELY. 155 Mbit/s optical wireless link using a bootstrapped silicon APD receiver. *Electronics letters*. 1994, vol. 30, no. 5, pp. 430–432. ISSN 0013-5194.

[2] CARRUTHERS, J. B. and J. M. KAHN. Angle Diversity for Nondirected Wireless Infrared Communication. *IEEE International Conference on Communications*. Atlanta: IEEE, 1998, pp. 1665–1670. ISBN 0-7803-4788-9. DOI: 10.1109/ICC.1998.683113.

[3] TANAKA, Y., T. KOMINE, S. HARUYAMA and M. NAKAGAWA. Indoor Visible Light Data Transmission System Utilizing White LED Lights. *IEICE transactions on communications*. 2003, vol. E86-B, no. 8, pp. 2440–2454. ISSN 0916-8516.

[4] DIMITROV, S. and H. HAAS. Information Rate of OFDM-Based Optical Wireless Communication Systems With Nonlinear Distortion. *Journal of Lightwave Technology*. 2013, vol. 31, no. 6, pp. 918–929. ISSN 2160-8881. DOI: 10.1109/jlt.2012.2236642.

[5] HUANG, X., S. CHEN, Z. WANG, J. SHI, Y. WANG, J. XIAO and N. CHI. 2.0-Gb/s Visible Light Link Based on Adaptive Bit Allocation OFDM of a Single Phosphorescent White LED. *IEEE Photonics Journal*. 2015, vol. 7, no. 5, pp. 1–8. ISSN 1943-0655. DOI: 10.1109/JPHOT.2015.2480541.

[6] HUANG, X., Z. WANG, J. SHI, Y. WANG and N. CHI. 1.6 Gbit/s phosphorescent white

LED based VLC transmission using a cascaded pre-equalization circuit and a differential outputs PIN receiver. *Optics Express*. 2015, vol. 23, no. 17, pp. 22034–22042. ISSN 1094-4087. DOI: 10.1364/OE.23.022034.

[7] MINH, H. L., D. O'BRIEN, G. FAULKNER, L. ZENG, K. LEE, D. JUNG, Y. J. OH and E. T. WON. 100-Mb/s NRZ Visible Light Communications Using a Postequalized White LED *IEEE Photonics Technology Letters,* 2009, vol. 21, iss. 15, pp. 1063–1065. ISSN 1041-1135. DOI: 10.1109/LPT.2009.2022413.

[8] O'BRIEN, D. C., H. LE MINH, G. FAULKNER, M. WOLF, L. GROBE, J. LI, and O. BOUCHET, Indoor Gigabit optical wireless communications: Challenges and possibilities. In: *International Conference on Transparent Optical Networks*. Munich: IEEE, 2010, pp. 1–6. ISBN 978-1-4244-7799-9. DOI: 10.1109/ICTON.2010.5549136.

[9] KIM, N.-T. Ultra-wideband bias-tee design using distributed network synthesis. *IEICE Electronics Express*. 2013, vol. 10, no. 15, pp. 1–8. ISSN 1349-2543. DOI: 10.1587/elex.10.20130472.

[10] KOUDELKA, P., J. LATAL, P. SISKA, J. VITASEK, A. LINER, R. MARTINEK and V. VASINEK. Indoor visible light communication: modeling and analysis of multi-state modulation. In: *Proceedings of Laser Communication and Propagation through the Atmosphere and Oceans, 9224*. San Diego: SPIE, 2015, pp. 1I-1–1I-8. ISBN 978-162841251-2. DOI: 10.1117/12.2063090.

[11] MARTINEK, R., J. ZIDEK and K. TOMALA. BER measurement in software defined radio systems. *Przeglad Elektrotechniczny*. 2013, vol. 89, iss. 2B, pp. 205–210. ISSN 0033-2097.

[12] STRATIL, T., P. KOUDELKA, J. JANKOVYCH, V. VASINEK, R. MARTINEK and T. PAVELEK. Broadband over Visible Light: High power wideband bias-T solution. In: *10th International Symposium on Communication Systems, Networks and Digital Signal Processing (CSNDSP)*. Prague: IEEE, 2016, pp. 1–5. DOI: 10.1109/CSNDSP.2016.7574002.

[13] MAHMOUD, H. A. and H. ARSLAN. Error vector magnitude to SNR conversion for nondata-aided receivers. *IEEE Transactions on Wireless Communications*. 2009, vol. 8, no. 5, pp. 2694–2704. ISSN 1536-1276. DOI: 10.1109/TWC.2009.080862.

[14] KOUDELKA, P., P. SOLTYS, R. MARTINEK, J. LATAL, P. SISKA, S. KEPAK and V. VASINEK. Utilization of M-QAM modulation during optical wireless Car to Car communication. In: *OptoElectronics and Communication Conference and Australian Conference on Optical Fibre Technology*. Melbourne: IEEE, 2014. pp. 452-454. ISBN 978-1-922107-21-3.

About Authors

Tomas STRATIL was born in 1990 in Olomouc, Czech republic. In 2015 He received Master's degree in optical communication from VSB–Technical University of Ostrava. His research interests include Visible light communication and Smart technologies.

Petr KOUDELKA was born in 1984 in Prostejov, Czech Republic. In 2006 received Bachelor's degree on VSB–Technical University of Ostrava, Faculty of Electrical Engineering and Computer Science, Department of telecommunications. Two years later he received on the same workplace his Master's degree in the field of Optoelectronics. In 2015 he successfully defended his dissertation thesis titled "Study of the Infoor Optical Wireless Network in the Visible Optical Radiation". He works as an Asistant Professor at VSB–Technical University of Ostrava since 2016. His current research interests include Wireless Optical Communications, Optical Access Networks and Smart City technologies.

Radek MARTINEK was born in 1984 in Czech Republic. In 2009 he received Master's degree in Information and Communication Technology from VSB–Technical University of Ostrava. Since 2012 he worked here as a Research Fellow. In 2014 he successfully defended his dissertation thesis titled „The Use of Complex Adaptive Methods of Signal Processing for Refining the Diagnostic Quality of the Abdominal Fetal Electrocardiogram". He became an Associate Professor in Technical Cybernetics in 2017 after defending the habilitation thesis titled "Design and Optimization of Adaptive Systems for Applications of Technical Cybernetics and Biomedical Engineering Based on Virtual Instrumentation". He works as an Associate Professor at VSB–Technical University of Ostrava since 2017. His current research interests include: Digital Signal Processing (Linear and Adaptive Filtering, Soft Computing - Artificial Intelligence and Adaptive Fuzzy Systems, Non-Adaptive Methods, Biological Signal Processing, Digital Processing of Speech Signals); Wireless Communications (Software-Defined Radio); Power Quality Improvement. He has more than 70 journal and conference articles in his research areas.

Tomas NOVAK was born in 1972 in Pribram, Czech Republic. In 1996 received Master's degree on VSB–Technical University of Ostrava, Faculty

of Electrical Engineering and Computer Science, Department of Electrical Engineering. Seven years later he received on the same workplace his Ph.D. degree in the field of Electric Light and Diagnostic. Now he works as an Associate Professor at the same university. His current research interests include Public Lighting, Lighting Pollutions, Interior Light Controlling and Smart City technologies.

Jan Latal - Miroslav Kralik - Zdenek Wilcek - Jakub Kolar - Josef Vojtech*

DEPLOYMENT AND MEASUREMENT OF QUALITY OF SERVICE PARAMETERS FOR TRIPLE PLAY SERVICES IN OPTICAL ACCESS NETWORKS

Broadband telecommunication networks are the future of communication and distribution of multimedia services. Thanks to the high transmission potential and capacity of optical fibres, the optical networks are predestined to be more widely used in telecommunications considering the higher data rates through Triple Play services. This paper describes the impact of selected quality parameters on multimedia services defined as Triple Play within an optical network based on the EPON standard. The Triple Play services are then evaluated with measuring instruments and software applications according to QoS requirements and using evaluation methods based on generally defined standards. These are mainly subjective (listening and conversational) and objective (MSE, PSNR, SSIM) methods, or parameters (MOS) and factors (bitrate, delay, packet loss rate, jitter, BER) that are defined for the respective service. The values measured during the experimental tests were related to the limiting parameters of optical topology based on EPON networks for individual services according to their QoS requirements and objective user evaluation.

Keywords: *Triple play, QoS, EPON, MSE, PSNR, SSIM, MOS, MPEG.*

1. Introduction

By using the broadband optical networks, telecom operators were allowed to distribute new types of multimedia services. To make it happen, however, it was necessary to find a suitable type of telecommunication system that would provide high transfer rates and allow reconfiguration. Nowadays, the role of this system is primarily played by optical networks. It was necessary to define the termination of the optical connection at the end customer according to FTTx (Fiber To The x), where x defines the termination of the optical line. FTTx networks are interconnected with PON (Passive Optical Network) optical access networks, which can be classified by their type into several kinds of EPON (Ethernet PON), GPON (Gigabit PON) or 10 GEPON (10 Gigabit EPON). They are going to gradually replace other technologies of access networks (e.g. xDSL-x Digital Subscriber Line, WiFi, etc.) and will probably very soon become the dominant access technology for access networks of the next generation – NGA (Next Generation Access). However, instead of using TDM (Time Division Multiplex) communication, the development of optical networks seems to head towards WDM (Wavelength Division Multiplexing), which brings new possibilities for increasing transmission capabilities and sharing multiple wavelengths between several end customers. There has also been a change of access to the media, as in passive optical networks, the TDMA (Time Division Multiple Access) time sharing approach is now being used more often, and new hybrid optical networks known as WDM-TDMA PON (Wavelength Division Multiplexing-Time Division Multiple Access Passive Optical Network) emerge with data rates of tens of Gbps. Moreover, the termination by FTTx enables to connect either directly to the home (FTTH, Fiber To The Home option) or to the office for corporate or office spaces (FTTO, Fiber To The Office option), but there is also the possibility of combined optical-copper connections using the current copper wiring in buildings, objects or larger blocks. These are the most often the FTTB (Fiber To The Building), FTTC (Fiber To The Curb) or FTTN (Fiber To The Node) variants. However, the main idea of the proposed solution of terminating all FTTx optical connections is the same. It is based on our intention to provide sufficient data rates for network endpoints and thus enable the end subscribers to access modern multimedia services. The one thing that the

* [1]Jan Latal, [1]Miroslav Kralik, [1]Zdenek Wilcek, [1]Jakub Kolar, [2]Josef Vojtech
[1]VSB-Technical University of Ostrava, Faculty of Electrical Engineering and Computer Science, Department of Telecommunications, 17. listopadu 15, Ostrava-Poruba, 70800, Czech Republic
[2]CESNET, a. l. e., Zikova 1903/4, 160 00 Prague 6 Czech Republic
E-mail: jan.latal@vsb.cz

aforementioned possibilities of using up-to-date services have in common is that we need a very careful and comprehensive design and planning of such network topology or infrastructure. It is necessary to pay attention to the fact that the given topology will be assembled not only from optical, but also metallic or wireless systems that must cooperate with each other. As a result, this can lead to lowered costs of both OPEX (Operating Expense) and CAPEX (Capital Expenditures) [1, 2].

By cooperation we mean the mutual synergy and adjustment, the management and reconfiguration options, and last but not least the available effective bandwidth for data transmission. Taking into account the different demands of the stated essential services within the "Triple Play" offer, it is also necessary to guarantee their QoS (Quality of Service) by establishing the necessary mechanisms for reserving sufficient transmission resources. For multimedia and voice services it will be necessary to solve the issues of delays in signal propagation, its fluctuations, etc. in a satisfactory manner [3 - 5].

The object of the following paper is to focus on Triple Play services and their requirements with regard to the parameters that have the largest impact on them, such as packet loss rate, delay, jitter and bandwidth, and also to demonstrate how these services behave in an experimental optical network [2, 3, 5]. All of these parameters are then related to the limiting values of the ODN (Optical Distribution Network), which is modified using fibres according to the ITU-T G.652 D standard and has a digital variable attenuator that can simulate longer and lossy transmission lines.

2. State of the art

Nowadays, the ever-growing demand for multimedia services and their development will, beside other things, require a thorough analysis to enable their smooth deployment and transmission, either within the existing or newly built networks. Optical networks serve as an example of a stable and high-quality system that represents the future for distribution of data communication. However, the deployment of multimedia services lies not only in using EPON, WDM-PON (Wavelength Division Multiplexing Passive Optical Network) or NGA/NGN (Next Generation Access/Next Generation Network) technologies, but also in GPON networks. GPON is a standard in compliance with ITU-T G.984 and is based on the use of GEM (GPON Encapsulation metod) protocol with ATM (Asynchronous Transfer Mode) cell support, while EPON (IEEE 802.3 ah) is based on the IP protocol. The GPON technology is very often deployed in Asian and American countries, where it is used for broadband access networks. GPON allows adjusting SBA (Static Bandwidth Allocation) or DBA (Dynamic Bandwidth Allocation), which is also used in EPON networks. However, neither of these networks defines the maximum possible parameters when achieving QoS for end units/users through Triple Play services [1, 2, 4, 6].

The research team of authors [7] has pursued the idea of improving the dynamic bandwidth allocation among differentiated services while maintaining QoS parameters defined for Triple Play in EPON networks through FIPACT (Frame-Oriented Interleaved Polling with Adaptive Cycle Time) algorithm [8]. To optimize the use of FQ-DBA (Frame-based QoS provisioning Dynamic Bandwidth Allocation) for allocating multimedia streams, a combination of EPON and WDM-PON is used while maintaining QoS parameters. Data streams for terminal units are preferentially defined using FQ-DBA in order to achieve sufficient bandwidth for a given service with respect to QoS.

In another paper, the team of authors discussed the possibilities of faster channel switching in EPON networks for IPTV (Internet Protocol Television) service using a new algorithm [9].

The IPTV and the use of IGMP (Internet Group Management Protocol) protocol in NGN will gain more importance. However, there are also associated problems with QoS and multicast distribution guarantees. The EPON networks meet the stringent demands on higher bandwidth and QoS, but they do not have satisfactory algorithms for allocating channels or streams among individual terminal units. For IPTV, the multicast mode needs a unique LLID (Logical Link Identificator) per channel for each ONU (Optical Network Unit) terminal unit. To prevent congestions of the network and OLT (Optical Line Termination) unit, a new type of algorithm for assigning LLID for individual IPTV channels has been designed [10].

Video quality analysis was researched in the study, comparing video codecs with relation to packet losses in the network. The results of them were artefacts in the video [11]. In other publications, however, the authors have focused on the impact of multiplying variable bitrate HD (High Definition) video streams with variable QoS settings. They have produced numerical simulations for various settings of packet loss, delay, jitter, bandwidth, etc. SwissQual VQuadHD and Telchemy VQMon applications were used for the evaluation [12].

Several research teams have also decided to simulate the behaviour of an EPON network with the Triple Play services implemented. They created an EPON network topology with a variable number of ONU terminal units and ODN network length of 0–65 km in a simulation environment. The results of the simulations confirm that the error rate changes with increasing number of terminal units, which affects the overall error rate of the given topology [13]. Apart from studying the ODN network range, other teams have also focused on the Q-factor, differential settings of system transfer rates from 2.5 to 10 Gbps with a variable number of terminal units connected in a network of 60–130. Based on simulations, it has been found that the EPON network can distribute sufficient transmission capacities even at 10 Gbps at a distance of up to 40 km [14].

3. Triple play

The term Triple Play service is well known nowadays, primarily when referring to multimedia services provided to ordinary customers. Triple Play is a term for a package of three services: high-speed data, internet television (IPTV) and internet telephony (VoIP, Voice over Internet Protocol) provided to the end user over a single connection. All of these services are distributed using the IP protocol (ISO/OSI model layer 3) in Ethernet network (ISO/OSI layer 2). The services are differentiated by the transport layer (ISO/OSI model layer 4). For transferring the data service, the TCP (Transmission Control Protocol) is used, which provides a reliable connection-oriented data transfer. In case of a data loss, a request to retransmit the lost data is sent. VoIP and IPTV multimedia services use the UDP (User Datagram Protocol), which provides connectionless and unreliable type of data distribution. In case of a data loss, there is no retransmission of the lost data. This approach eliminates delays, but degrades the service. Apart from the delay, other important parameters that affect the quality of multimedia services are also the bandwidth, packet loss rate and jitter (delay fluctuations) [15]. Another parameter that also has an impact on the distribution of Triple Play services is OoS (Out of Sequence), which indicates wrong order of data reception, i.e. when the data is received in an order that is different from the order in which it was originally sent. This phenomenon can occur when the data travels through different paths in the network. The QoS (Quality of Service) term is defined with the multimedia services and describes the technical part that must be maintained for the right functionality of the individual services. Based on the requirements, the services can be classified with regard to the transmission type [2]. Therefore, the distribution of Triple Play services has much higher demands on the quality of the distribution infrastructure when compared to the conventional data transfers. The applied technology must provide enough capacity to support the QoS mechanisms (CoS/DiffServ, etc.) that will allow the distribution of services with different requirements for bandwidth, sufficient level of QoE (Quality of Experience), security and reliability.

3.1 Factors affecting the quality of audio and video services

There are numerous of factors that affect multimedia services and have a negative effect, causing gradual deterioration in the quality of the individual audio and video services. Applications used for voice, video and data transmission need more bandwidth for the transfer and they are sensitive to delay and packet loss. As soon as these parameters are exceeded, the service becomes unusable. During the transmission of data, there can be several possible causes of problems on the way from the sender to the recipient. We talk about latency, packet order, delay, bitrate, delay fluctuation (jitter) and packet loss [2].

3.2 Methods for determining the quality of VoIP service

The methods for evaluating speech quality can be classified into two basic groups: the subjective and the objective evaluation methods. During our measurements we were focused on subjective as well as on objective methods for evaluating the quality of VoIP. They will be mentioned and described in the following chapters.

3.2.1 Subjective VoIP service quality evaluation

The conversational methods (CQ – Conversational Quality) are laboratory simulations where two subjects communicate via a phone call and evaluate the transmission quality of the call signal. A third person measures the test conditions. The evaluation uses the MOS (Mean Opinion Score) rating scale. The listening methods (LQ – Listening Quality) do not reflect reality as much as the previous type, but they are easier. They consist of playing speech signals to the subject who evaluates them using multiple possible methods (ACR - Absolute Category Rating, QRDM - QR-decomposition with M-algorithm, DCR - Degradation Category Rating, CCR - Comparison Category Rating). The MOS rating parameter was created based on the ITU P.800 recommendation. It is a part of ACR family – the Absolute Category Rating, based on the comparison of a received signal with the reference signal. The result is obtained by averaging the subjective user opinions about the perceived voice [2].

3.2.2 Objective VoIP service quality evaluation

Here, the statistical evaluation of mathematical models that simulate the human auditory system is used. Among the best algorithms are PAQM (Perceptual Audio Quality Measure), PSQM (Perceptual Speech Quality Measure), NMR (Noise-to-Masked-Ration, PERCEVAL (Perceptual Evaluation), DIX (Distrubance Index), OASE (Objective Audio Signal Evaluation) and POM (Perceptual Objective Measure). We can also mention a metric one which, apart from factors affecting quality, also takes user perception into account. This metric is called R-factor and is used in a calculation model known as the E-model. This model is described in detail in the recommendation G.107. The basic formula for calculating the value of R-factor is [16]:

$$R = R_0 - I_s - I_d - I_e + A \quad (1)$$

where R_0 is the basic signal-to-noise ratio, I_S is the simultaneous interference factor defined as the sum of all deterioration

effects (noise from the surroundings, etc.) which can occur simultaneously with voice transmission, I_d represents all deteriorations caused by the delay of voice propagation, I_e (also labelled as $I_{E\text{-}EFF}$ in the literature) is a factor representing the degradation of quality caused by the packet loss, and A is an advantage factor that depends on the concentration of the listener (from 0 to 20 depending on the codec) [2]. The above mentioned calculation also includes a set of recommended values which allows to simplify the calculations to suit the packet networks. Among the important parameters with regard to QoS in packet-based networks are the network delay, jitter and packet loss. These parameters are included in two of the parameters mentioned in the R-factors calculations, namely in I_d and I_e (or $I_{E\text{-}EFF}$) [3, 5].

$$I_d = I_{DTE} + I_{DD} \tag{2}$$

The I_{DTE} parameter represents the factor of impairment caused by echo (echo cancellation has been solved in ITU-T G.168 recommendation). The I_{DD} factor represents the factor of interference caused by a too long transmission delay. By keeping all the default values in R-factor calculation we obtain the final value of 93.35. The value of 93.35 can be achieved only in ideal environment without any disturbance. In order to meet the user expectations, it is necessary to get a value of 70 or more. A simplified R-factor calculation uses this final form:

$$R = 93.35 - I_d - I_e \tag{3}$$

The resulting R-factor is a numerical value that usually lies between 15–94, while the value above 70 is considered to be acceptable.

3.3 Methods for determining the quality of IPTV

There are recommendations for evaluating image and video signal quality available, e.g. ITU-T P.910. Subjective measurements of image and video signal quality are based on the human perception. The advantage of this measurement is that people can describe the image according to what they really see and therefore suppress information that is imperceptible to the human eye. The subjective measurements are influenced by a number of factors which makes the repeatability of these subjective measurements difficult. There are several approaches to IPTV quality measurements, for instance MSE, PSNR, SSIM, MDI (Media Delivery Index) or MPQM (Moving Pictures Quality Metric) to name some of the objective methods. The group of subjective methods for evaluation of IPTV quality include MOS, DSCQS (Double Stimulus Continuous Quality Scale), DSIS (Double Stimulus Impairment Scale), and ACR (Absolute Category Rating). Within experimental measurements we were primarily focused on the objective methods of IPTV quality evaluation, namely on the MSE, PSNR and SSIM described in more detail below, and supplemented them with real measured values in later chapters [2, 17, 18].

3.3.1 MSE (Mean Square Error)

MSE represents the mean square error between the received and original video signals. The following formula is used for the calculation:

$$MSE = \frac{1}{M \times N} \Sigma_{j=0}^{M-1} \Sigma_{j=0}^{N-1} (x_{ij} - y_{ij})^2 \ [-] \tag{4}$$

where x is the original image, y is the received image, elements i and j are the elements of the image matrix, M is the image height in pixels and N is the image width in pixels [2].

3.3.2 PSNR (Peak Signal to Noise Ratio)

PSNR is the ratio between the highest values relative to the MSE and is expressed by the following formula:

$$PSNR = 10 \times \log \frac{m^2}{MSE} = 20 \times \log_{10}(m) - 10 \times \log_{10}(MSE) \ [dB] \tag{5}$$

where m is the maximum value a pixel can get [2].

3.3.3 SSIM (Structural Similarity Index)

The SSIM parameter takes the human visual system into account. It measures the similarity between two images. The SSIM has been developed to improve conventional metrics such as MSE and PSNR that were proven to be inconsistent with human perception. The reference values lie within the interval of <0,1>, where 0 represents no relationship to the original image and the value of 1 is reached when two identical pictures are compared.

$$SSIM(x,y) = [l(x,y)]^{\alpha} [c(x,y)]^{\beta} [s(x,y)]^{\gamma} \tag{6}$$

The term *l(x, y)* is used to compare the signal luminance, the term *c(x, y)* compares the signal contrast and the term *s(x,y)* is used to measure the structural correlation, which is calculated from the following relations:

$$l(x,y) = \frac{2\mu_x\mu_y + c_1}{\mu_x^2 + \mu_y^2 + c_1} \tag{7}$$

$$l(x,y) = \frac{2\sigma_x\sigma_y + c_2}{\sigma_x^2 + \sigma_y^2 + c_2} \quad (8)$$

$$l(x,y) = \frac{\sigma_{xy} + c_3}{\sigma_x\sigma_y + c_3} \quad (9)$$

where μ_x and μ_y represent the average of x and y samples, C_1, C_2 are constant and σ_x and σ_y represent the dispersion of x and y samples [2].

4. Carrying out experimental measurements of triple play services in EPON network

Here we come to the real results that were obtained in the course of measuring the effects of ODN limiting parameters on the built optical topology for different types of Triple Play services. However, the main motive is to demonstrate and verify the practical impact of the main network parameters on the behaviour of multimedia as well as traditional data services. This chapter gives an overview of the impact of QoS parameters on Triple Play services within the EPON network (EPON type 2). The introduction provides a description of the used experimental topology and devices designed to simulate Triple Play services in a network, and then a set of tests and their results. The processed measured values are a subject to evaluation through objective tests based on mathematical foundations described above.

4.1 Measurement of triple play services in EPON network

The basis for the measurement was the topology shown in Figure 1, using a core of OLT EPON type 2 unit with the following basic parameters: the range of about 20 km, the maximum defined split ratio of 1:32 at the used wavelengths 1310 nm (upstream), 1490 nm (downstream) and a transmission rate of 1 Gbps or 1.25 Gbps, where 250 Mbps is used for overhead needed for data transmission and administration [1]. Among other parts was an optical line with the length of 5.773 km made of an ITU-T G.652 D fibre and six ONT/ONU terminal units connected through a symmetric optical splitter (1:7 ratio) having an insertion loss of 8 dB. Additionally, the tested topology was supplemented by EXFO FVA-60B device that was supposed to simulate the ODN network range by increasing insertion loss into the line. The topology was also supplemented by a Simena NE1000 network element for impairment creation, Abacus server used as an IPTV server, a PC (Acer laptop) with MSU Video Quality Measurement Tool application, IP phones (Grandstream GXV3140) to create VoIP service and finally a EXFO AXS200/625 measuring instrument to evaluate qualitative parameters of the multimedia services.

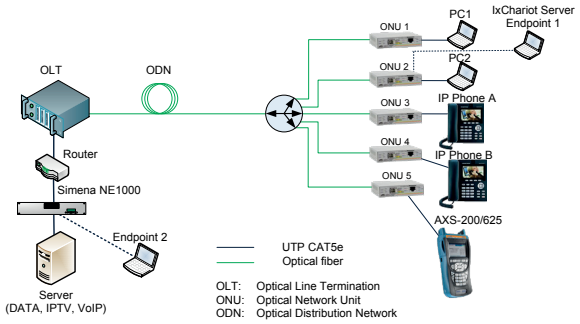

Fig. 1 The topology for Triple Play services deployment and for monitoring the impact of QoS parameters on the services

The Triple Play services were enabled by an Abacus server on which the individual services were implemented, and the user side used laptops or IP phones. The tested topology was also supplemented by a PC with the IxChariot tool (and also serving as an Endpoint 1 for this tool) and by another PC which worked as an Endpoint 2. This topology extension marked with a dashed line in the diagram enabled us to define the quality of VoIP services and to evaluate it. As our goal was to determine the limiting values of the optical distribution network (ODN) and its impact on the Triple Play multimedia services, we have defined the values at which the given topology was still fully functional without communication breakdowns or increased error rates. During the experimental measuring it has been proven that with an additional insertion loss in the line created by a variable digital attenuator, the given topology was able to bridge a gap of 21.95 dB at the wavelength of 1310 nm. It should be noted that the value is related primarily to the ONU unit, as the OLT unit was still able to transmit with 32.2 dB insertion loss at the wavelength of 1490 nm. However, this is caused by the fact that the transmitter located in the OLT unit has more power than the source of radiation used in the ONU unit.

For our purposes, the service for VoIP was distributed via IxChariot. The codecs used were G.711 μ-law, G.723.1 ACELP (Algebraic Code-Excited Linear Prediction), G.729. These types of codecs are often used for VoIP communications and compression of audio data. The most bandwidth/bitrate-demanding codec is G.711 μ-law, which requires 64 kbps. The G.711 standard was designed in 1992 and is intended for PSTN networks. G.723.1 – this standard is intended for multimedia applications and includes two speech coders. One of them uses a transmission rate of 5.3 kbps and the other one a transmission rate of 6.4 kbps. The distinctions between them are in different codebooks with different excitation sequences. The frame size is 30 ms, the delay due to frame overlapping is 7.5 ms, and the total delay of the coder is 67.5 ms. The G.729 standard has been developed primarily for mobile networks applications. A coder based on G.729 has a low bit rate of 8 kbps. The frame size was set to be 10 ms, which allowed reaching a compromise between the

quality of the reconstructed speech signal and the computational complexity of the coding algorithm. The delay caused by frame overlapping (lookahead) is 5 ms and the total delay is 25 ms. Nowadays, however, we can find more advanced types of codecs [2, 16].

The distribution of video streams was prepared using VLC Streamer and Abacus server with three main HDTV (High-definition television) and SDTV (Standard-definition television) video samples and different types of MPEG-2 (Moving Picture Experts Group) or MPEG-4 compliant compression codecs. MPEG-2 is the older of the codecs and was developed in 1994. Its predecessor is the MPEG-1 format and its more advanced technological successor is the MPEG-4 format. MPEG-2 is the standard format used for storing and transferring video on DVDs or for the distribution of DVB-T (Digital Video Broadcasting - Terrestrial) digital television signal. Applications that require real-time MPEG-2 video compression and decompression are much more demanding in terms of the computing capacity of a processor than with the MPEG-1 format. The difference between MPEG-1 and MPEG-2 formats is that the latter can work with the so-called VBR (Variable Bit Rate). MPEG-2 was developed for the resolution of 720×576 pixels which corresponds to SDTV. MPEG-4 is a collection of patented methods that define the compression and storage of audio and video data. It was introduced to the world in 1998 and it represented a group of standards for encoding audio, video and related technologies. It was formally issued by ISO/IEC MPEG as an ISO/IEC 14496 standard. Many features of the MPEG-4 standard are defined as optional. MPEG-4 is a standard which is still being developed, especially some of its parts. The new compression method according to H.264 for MPEG-4 version 10 will also come in handy to those who need to effectively archive or download/upload video recordings. The H.264 codecs allow reducing the capacity demands for the transmission of video data streams to one half or one third when compared to MPEG-2, which makes them an ideal type of codec for any kind of broadcast. The following chapters state all measurement methodologies for Triple Play services in EPON networks [2, 17, 18].

4.2 Measuring IPTV using EXFO AXS 200/625

The first step of the experiment with the Triple Play services implemented in the EPON network was measuring the data rates of three different video samples. These samples were distributed via a network established from a server to a terminal unit represented by EXFO AXS 200/625 analyser. The analyser performed detailed measurements of the impact of the loss rate in the selected video samples on the limit value of the experimental topology with EPON. In Table 1 we can see the test samples used for measuring the change of transmission rate and the impact of

Samples used for transmitting in the analysis with AXS 200/650 Table 1

Samples	File type	Size [MB]	Average bitrate [kbps]	Frames per second	Resolution	Codec	Length
MPEG-2 HDTV	MPEG	374	9 843	29.970	1 280×720	MPEG2	5 min 9 s
MPEG-4 HDTV	AVI	420	11 456	29.970	1 920×1 080	MPEG4	5 min 7 s
MPEG-2 SDTV	MPEG	136	1 154	25.000	720×480	MPEG2	14 min 46 s

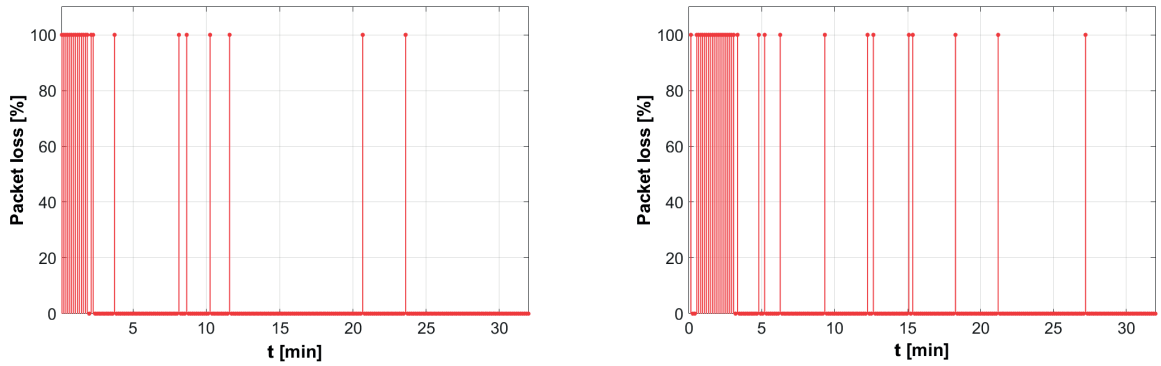

Fig. 2 MPEG-2 HD (left) and MPEG-4 HD (right) video

transmission time on the error rate (packet loss) for the limiting settings of the experimental topology with EPON.

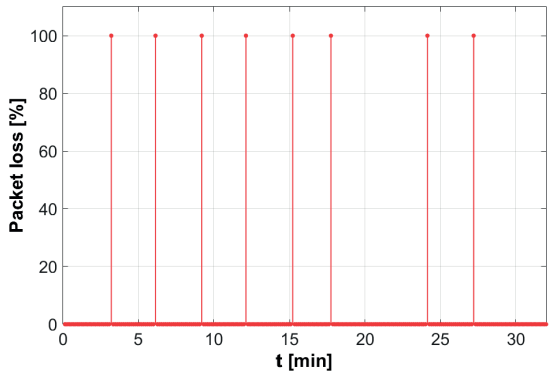

Fig. 3 MPEG-2 SD video

Figures 2 and 3 present the effect of the transfer rate on the error rate, i.e. packet loss. The length of the measurement was 30 minutes (to be more specific, although the test samples are shorter than the test period, they were played in a loop) and the network throughput was changed from 10 Mbps to 100 Mbps in steps of 10 Mbps every 3 minutes. The EXFO AXS 200/625 analyser evaluated the error rate using a 1/0 method, where "1" means there was an error and "0" means there was no error. We can see that the transfer rate influenced the error rate primarily in the HD video samples. The occurrence of errors depended on the video *bitrate* and the large occurrence of errors took place only during the first step (the first 3 minutes) at a speed of 10 Mbps, which confirms the demand for a minimum data rate defined for a particular video format in QoS [2]. In the subsequent steps, the errors in the HD video samples occurred just rarely. For the MPEG-2 SD sample, the errors occurred rarely from the beginning to the end of the experimental measurement.

4.3 MSU video quality measurement tool – IPTV service

For the next step of testing the IPTV services, the MSU VQMT software application was used to evaluate and analyse the objective methods. Using a Simena NE1000 network emulator we modified the critical parameters of the network that in turn affected the IPTV. Three basic types of video samples (see Table 2) were used for experimental measuring, which are the types currently used for distributing IPTV to its customers.

The effect of bitrate on the objective methods MSE, PSNR and SSIM can be seen in Figs. 4-6. Figure 4 shows the plot of the MSE objective method that represents the mean square error between the original signal and the signal received on the other side of the network. Deterioration can be seen in MPEG-2 HD and HD MPEG-4 video samples at speeds lower than 20 Mbps. It comes from their demand for bitrate which for the given video resolution varied up to a maximum of 20 Mbps and did not exceed this value. The MPEG-2 SD sample shows no errors, even when it requires a bitrate lower than 10 Mbps. The PSNR objective method is similar.

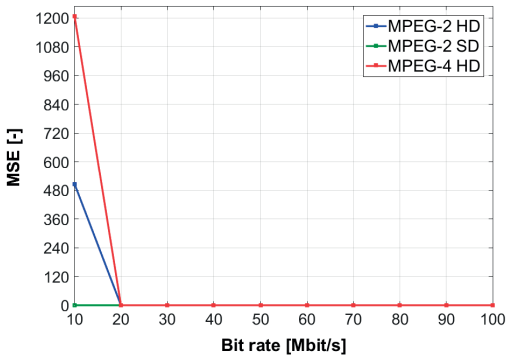

Fig.4 The effect of bitrate on MSE

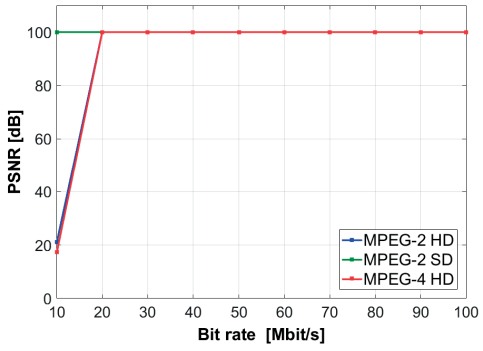

Fig. 5 The effect of bitrate on PSNR

Video samples used for analysis by the objective methods with the VQMT MSU application — Table 2

Sample	File type	Size [MB]	Average bitrate [kbps]	Frames per second	Resolution	Codec	Time
MPEG-2 HDTV	AVI	26.7	10 427	29.970	1 280×720	MPEG-2	20 s 19 ms
MPEG-4 HDTV	AVI	24	9 061	29.970	1 920×1 080	MPEG-4	20 s 89 ms
MPEG-2 SDTV	AVI	5.9	2 132	25.000	720×480	MPEG-2	20 s 88 ms

Figure 6 shows plots of the SSIM objective method, which is based on the MSE and PSNR methods. The results of the measurement are very similar. Slightly worse results were obtained for the MPEG-4 HD video sample when the bitrate was 10 Mbps.

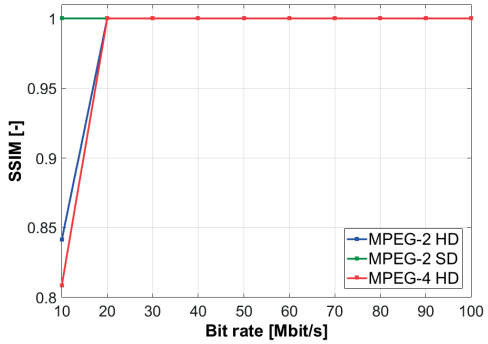

Fig. 6 The effect of bitrate on the SSIM

Figure 7 plots the effect of error rate on the MSE and PSNR objective methods. The worst results were obtained for the MPEG-4 HD sample and the results were very good for the less demanding video represented by MPEG-2 SD. The effect or change of the values for each of the objective method appears for BER = 10^{-8} or lower.

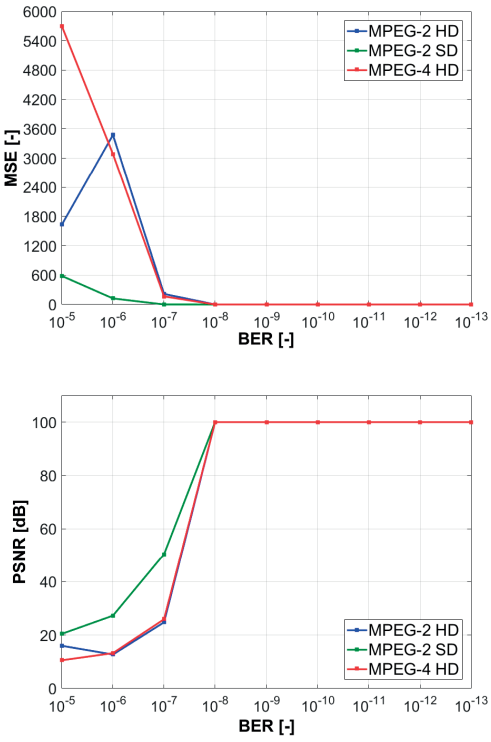

Fig. 7 The effect of BER on MSE (top) and PSNR (bottom)

Figure 8 shows the effect of the error rate on the SSIM objective method. The results are similar as for the previous methods. Here again the MPEG-4 HD sample gives the worst values and the effect can be seen for BER values below 10^{-8}.

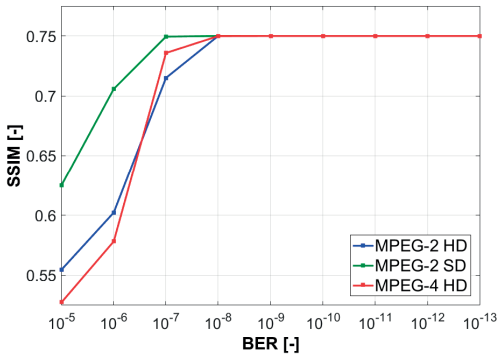

Fig. 8 The effect of BER on SSIM for the tested video samples

Figures 9 and 10 show the impact of packet loss rate on the objective methods MSE, PSNR and SSIM. For these parameters it is possible to see the effect starting from the smallest set values. We can also see relatively large fluctuations of the values, which may be caused by the set dynamic packet loss rates at the individual percentage values. The real measurements show that MPEG-4 HD has the worst results and by contrast, the best results can be seen for the MPEG-2 SD sample.

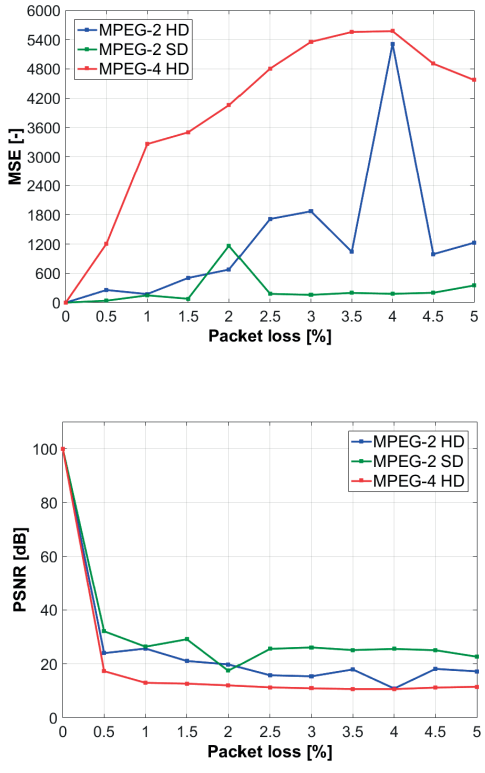

Fig. 9 Impact of packet loss rate on MSE (top) and PSNR (bottom)

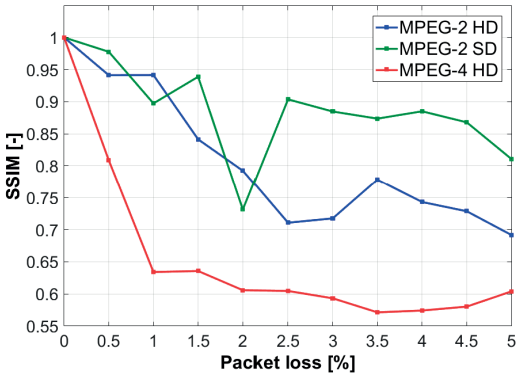

Fig. 10 Impact of packet loss rate on SSIM

By using the quoted results and our observations of the video samples we can evaluate the impact of the individual parameters on the video quality. For the BER (Bit Error Ratio) parameter, the quality is deteriorated for values of 10^{-7}. The packet loss rate parameter affects the video from the lowest set value, but the difference can be seen in MPEG-2 SD and MPEG-2 HD, where MPEG-2 HD with high loss rate (about 3 %) is hard to watch, while MPEG-2 SD image is much better to distinguish and watch. The difference can also be seen for admissibility, which has an impact on the format and resolution of the video. The effects of QoS parameters such as *jitter* and delay was also observed. The requirements state the maximum value of *jitter* to be less than 50 ms and delay under 200 ms. During testing, these parameters were set at much higher values, yet there was no impact on the video quality. However, they did cause a delay of the received audio signal from the original transmitted one.

4.4 IxChariot – VoIP service

The evaluation of VoIP call quality has been carried out mainly on the G.711 μ-law codec, which is supposed to be the most often used codec by voice service providers. A comparison with other codecs (G.723.1 ACELP, G.729) has also been made. The main parameters by which the voice call was evaluated were MOS and R-factor values, which are related and can be compared with each other. To evaluate the VoIP service, we have used the IxChariot program that allows the simulation of calls with various settings. We have evaluated the effects of several critical parameters (bitrate, jitter, BER, delay and packet loss rate) that have the greatest impact on the quality of the service. The values obtained from the experimental measurements are shown in Figs. 11 - 13.

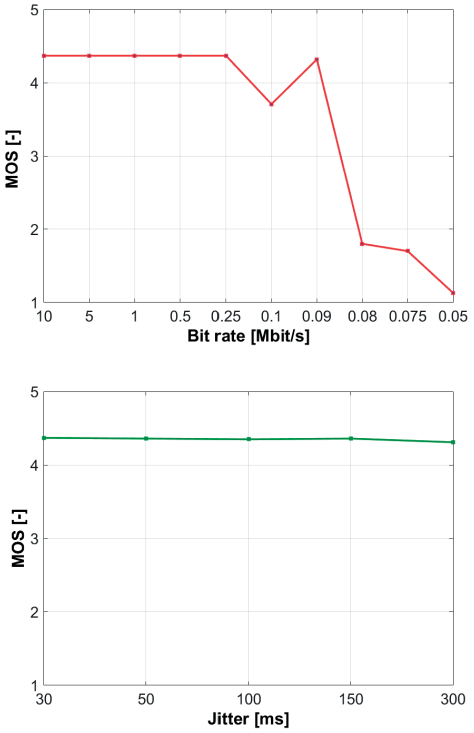

Fig. 11 The impact of the bitrate (top) and jitter-u (bottom) on the call quality (MOS) for VoIP codec G.711

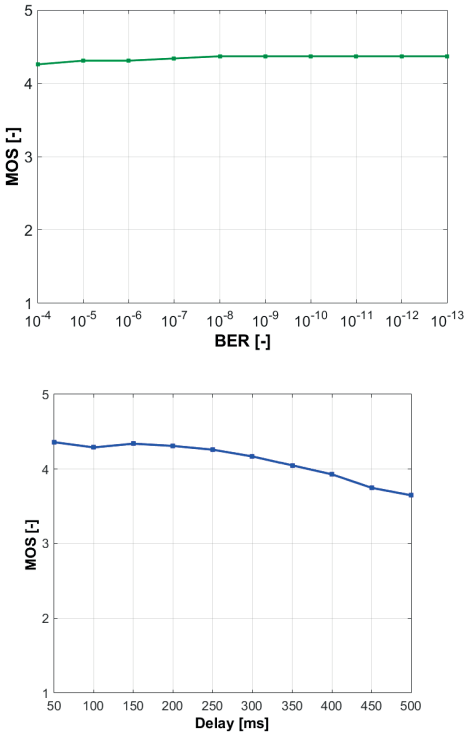

Fig. 12 The impact of the BER (up) and delay (down) on the call quality (MOS) for VoIP codec G.711

Figures 11 and 12 show the impact that the changes of individual parameters have on the call quality for codec G.711 μ-law. Parameters such as delay, jitter and error rate have almost no effect on the call quality, even when they are set above the values defined as maximum for QoS requirements in ITU-T. This was caused by the fact that the network load was low during the measurement as there were no running services for IPTV or data transmissions. The effect on the MOS value is apparent for the bitrate change (see Fig. 11) when the value was set to 0.09 Mbps or less. These are low bitrate values, but the given topology can cover them without major problems. The last parameter also has the largest impact – it is the packet loss rate. That is why this parameter was also tested on other types of codecs. Apart from G.711 μ-law these were G.729 and G.723.1 ACELP.

Figure 13 shows that the highest impact of packet loss rate can be seen with the G.711 μ-law codec, for which the MOS value dropped from 4.2 down to 1.73, which is already a value showing unsatisfactory to poor call quality, while the limiting value of MOS for a satisfactory call is 3 or above. For G.729 and G.723.1 ACELP codecs the MOS value turned out to be just under the limit of 3 (the G.723.1 ACELP codec), where these codecs reach the limits of acceptability for call quality at the packet loss rate of 5 %. The codec that is most resistant against packet loss is G.729.

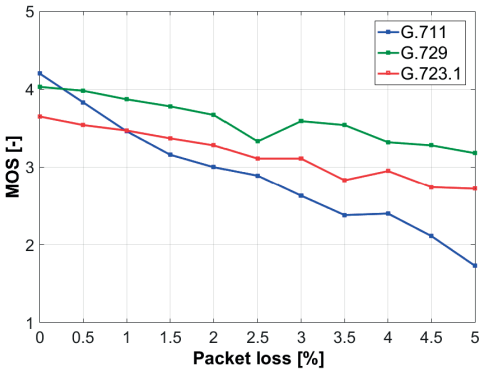

Fig. 13 The impact of packet loss rate on VoIP call quality (MOS) for individual codecs

4.5 The impact of QoS parameters – data service

The impact of QoS on the data transfer was recorded using the BWMeter software application. It allowed us to record the actual transfer rates in both directions in one second intervals. The data was transferred using a created data server from which the data was downloaded and on which it was also uploaded. The data sample used had a size of 18100 Mb. During the measurement we observed the extent of limitations that the error rate and packet loss rate parameters had on the data transfer service.

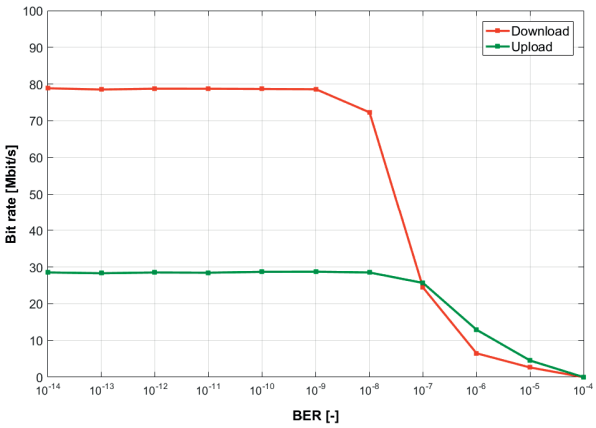

Fig. 14 The effect of BER on the transfer rate – download/upload

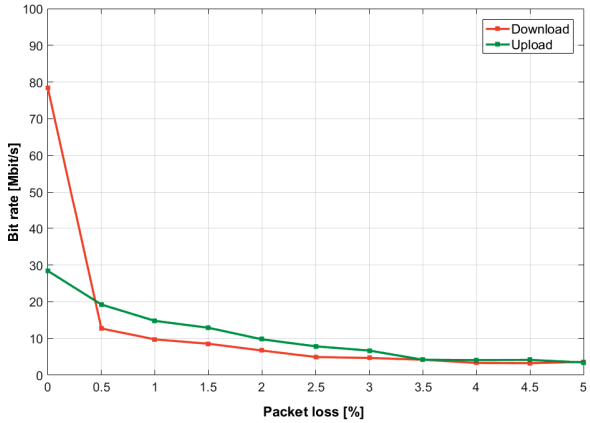

Fig. 15 The effect of packet loss rate on the transfer rate – download/upload

In Fig. 14 we can see the effect that the error rate parameter has on the data transfer. The measurements show that up to BER values of 10^{-9}, the transfer is error-free, but when the values go lower, a drop in transfer rates is apparent in both directions. The complete breakdown occurs at the value of 10^{-4}. Figure 15 describes the effect of the packet loss rate on the data transfer. We can see that the effect of this parameter is more noticeable even at the first step with a packet loss rate of 0.5 %, when there is a significant decrease in transfer rates. Increasing the packet loss rate further only causes moderate constant descent of the transfer rate in both directions. The connection still works until the last step of 5 %, where the value is around 3.6 Mbps.

5. Conclusion and evaluation

The results of the experimental measurements demonstrate the characteristics of the EPON network that shows itself to be a suitable candidate for the implementation into the infrastructure

with regard to Triple Play services deployment by internet service providers. The paper introduces various measurement options that demonstrate the impact and limits of the parameters affecting the multimedia services and methods for evaluating the quality of Triple Play services. The results show that the most appropriate format for distribution in IPTV services is MPEG-2 HD, which is a sort of compromise between quality and network requirements. For VoIP voice services, the most often used codec is G.711 μ-law. However, in the last test of packet loss rate, the G.729 codec that requires less bitrate has shown better results.

For data services, the essential parameter for an end user is the bandwidth or bitrate, but the error rate or packet loss rate in the network are also quite important. From a global viewpoint, the EPON standard and its extensions are a great choice, as they have excellent transmission characteristics and offer to set up QoS policies in the network for individual multimedia services. The main contribution of this paper is the way in which it is possible to deploy and subsequently evaluate the behaviour of a network based on the EPON standard and also the deployment of Triple Play services with regard to the evaluation of quality and their demands. The future work will be primarily focused on creating new types of NGA/NGN networks and setting up QoS policies with regard to the parameters critical for the Triple Play services. We will also look at the possibilities of adding new video formats (e.g. UHD, h.265, VP9) [19, 20] or higher transmission rates that will be offered to end users by their providers together with other services (Smart applications, etc.).

Acknowledgement

The research described in this article could be carried out thanks to the active support of the projects No. SP2017/79, SP2017/97, VI20172019071, CZ.1.07/2.3.00/20.0217, CESNET 614R1/2017. The presented research has been supported by project E-infrastructure CESNET – modernization, registration no. CZ.02.1.01/0.0/0.0/16 013/0001797.

References

[1] LAM, C. F.: *Passive Optical Networks: Principles and Practice.* Elsevier,Boston, p. 324, 2007.

[2] HENS, F. J., CABALLERO, J. M.: *Triple Play: Building the Converged Network for IP, VoIP and IPTV.* Wiley, Hoboken, p. 401, 2008.

[3] FRNDA, J., VOZNAK, M., SEVCIK, L.: Impact of Packet Loss and Delay Variation on the Quality of Real-Time Video Streaming. *Telecommunication Systems,* 62(2), 265-275, 2016.

[4] IFTIKHAR, R., KALEEM, I. M., ABDULLAH, S. M.: *Triple Play Services over EPON Triple Play Services over Ethernet-Passive Optical Networks.* IEEEP Symposium, EIR-16(5), Pakistan, 2010.

[5] FRNDA, J., VOZNAK, M., FAZIO, P., ROZHON, J.: *Network Performance QoS Estimation.* Intern. Conference on Telecommunications and Signal Processing (TSP 2015), Czech Republic, 2015.

[6] SULTAN, D. M. S., TASLIM, MD. A.: GPON, The Ultimate Pertinent of Next Generation Triple-Play Bandwidth Resolution. *Journal of Telecommunications and Information Technology*, 2, 53-60, 2011.

[7] LIN, H. –T., LAI, CH.-L., WANG, T.-SH, HUANG, Y.-CH.: *Supporting Triple-Play Services with Private Networking over WDM EPONs.* Intern. Symposium on Communications and Information Technologies (ISCIT 2014), South Korea, 2014.

[8] LIN, H.-T., LAI, CH.-L., LIU, CH.-L.: Design and Analysis of a Frame-Oriented Dynamic Bandwidth Allocation Scheme for Triple-Play Services over EPONs. *Computer Networks*, 64, 339-352, 2014.

[9] NIE, Y., YOSHIUCHI. H.: *A Fast Channel Switching Method in EPON System for IPTV Service*.Springer, Berlin Heidelberg, p. 280, 2009.

[10] HWANG, I.-SH., NIKOUKAR, A.-A., LIEM,A. T., CHEN, K.-CH.: *A New Architecture for Multicasting Live IPTV Traffic in Ethernet Passive Optical Network.* Intern. Conference on Electronics, Computer and Computation (ICECCO 2013), Turkey, 2013.

[11] YIM, CH., BOVIK, A. C.: Evaluation of Temporal Variation of Video Quality in Packet Loss Networks. *Signal Processing: Image Communication*, 26(1), 24-38, 2011.

[12] MAKOWSKI, P.: Quality of Variable Bitrate HD Video Transmission in New Generation Access Network. *Journal of Telecommunications and Information Technology*, 1, 21-26, 2014.

[13] KOCHER, D., KALER, R. S., RANDHAWA, R.: Simulation of Fiber to the Home Triple Play Services at 2Gbit/s using GE-PON Architecture for 56 ONUs. *Optik*, 124(21), 5007-5010, 2013.

[14] SINGH, S.: Performance Evaluation of Bi-Directional Passive Optical Networks in the Scenario of Triple Play Service. *Optik*, 125(19), 5837-5841, 2014.

[15] VODRAZKA, J., LAFATA, P.: Transmission Delay Modelling of Packet Communication over Digital Subscriber Line. *Advances in Electrical and Electronic Engineering, 11*(4), 260-265, 2013.

[16] KOVAC, A., HALAS, M.: E-Model MOS Estimate Precision Improvement and Modelling of Jitter Effects. *Advances in Electrical and Electronic Engineering*, 10(4), 276-281, 2012.

[17] BIENIK, J., UHRINA, M., VACULIK, M., MIZDOS, T.: Perceived Quality of Full HD Video - Subjective Quality Assessment. *Advances in Electrical and Electronic Engineering*, 14(4), 437-444, 2016.

[18] UHRINA, M., HLUBIK, J., VACULIK, M.: Correlation between Objective and Subjective Methods Used for Video Quality Evaluation. *Advances in Electrical and Electronic Engineering, 11*(2), 135-146, 2013.

[19] UHRINA, M., FRNDA, J., SEVCIK, L., VACULIK, M.: Impact of H.264/AVC and H.265/HEVC Compression Standards on the Video Quality for 4K Resolution. *Advances in Electrical and Electronic Engineering*, 12(4), 545-551, 2014.

[20] UHRINA, M., BIENIK,J., VACULIK, M.: Impact of GoP on the Video Quality of VP9 Compression Standard for Full HD Resolution. *Advances in Electrical and Electronic Engineering*, 14(4), 445-452, 2016.

Purposeful Suppression and Reconstruction of White Light from LED for Improvement of Communication Properties

Jan VITASEK, Jan LATAL, Tomas STRATIL, Stanislav HEJDUK, Ales VANDERKA, Lukas HAJEK, Jakub KOLAR

Department of Telecommunications, Faculty of Electrical Engineering and Computer Science, VSB–Technical University of Ostrava, 17. listopadu 15, 708 00 Ostrava, Czech Republic

jan.vitasek@vsb.cz, jan.latal@vsb.cz, tomas.stratil@vsb.cz, stanislav.hejduk@vsb.cz, ales.vanderka@vsb.cz, lukas.hajek@vsb.cz, jakub.kolar.st@vsb.cz

DOI: 10.15598/aeee.v17i1.2671

Abstract. *Visible Light Communication (VLC) technology uses white Light Emitting Diodes (LED) for providing illumination and communication at the same time. White LEDs have excellent illumination properties but their communication properties need improvement. This article proposes a way how to evade the communication limitations of white LEDs. A part of original white LED spectrum is suppressed by an optical filter. Then the suppressed part is replaced by another LED. The correct choice of suitable LED enables to reconstruct the original spectrum. This solution removes the limitations because the white LED emits continuously. Data are carried by the communication LED only. The evaluation of reconstruction of original white light is measurement of the colour coordinates x and y. Furthermore, the communication properties of this transmitter were tested and obtained results are shown in this paper. EVM parameter was measured.*

Keywords

CIE coordinates, communication via LEDs, EVM, MQAM, VLC, white light.

1. Introduction

One of research directions in optical communications is the Visible Light Communication (VLC). The VLC technology joins together two functions, communication and illumination [1], [2], [3], [4] and [5]. The VLC is mainly used indoor and it has the potential to partially replace the radiofrequency communication (Wi-Fi). This replacement is caused by several factors [6]:

- Dwindling RF spectrum: the radiofrequency spectrum is limited, its usage is regulated due to interferences, pollution and efficient spectral usage. It is cheaper for mobile operators to buy spectrum than building more base stations for capacity increasing. Moreover, it reduces the chance for future operators to enter the market. The requirements for wireless data transmission are constantly increasing, therefore the radio frequency spectrum becomes congested. There have been developments to use the Terahertz frequency range between the RF and microwave spectrum, but it would mean creating an entirely new class of infrastructure compatible with the wavelength band. On the other hand, visible light has 10 000 times greater spectrum than radio waves [7] and [8].

- Capacity: Mobile data will grow 6.3 times between 2013 and 2018 and the growth will be strongest outside Europe and North America [9] and [10]. Thanks to the massive increase in data usage, mobile operators focus on public Wireless Fidelity (Wi-Fi) and other alternative technologies. The growth of mobile data usage is obvious.

- Interference: VLC is safe and does not cause any interference with RF waves. Thus this technology is perfectly suitable for communication in hospital, industrial and aerospace applications [11].

- Security: RF waves pass through walls and could be received by a third person, are susceptible to snooping. Light has clearly defined boundaries and defined coverage zones with enhanced security for VLC.

- Safety: in illumination conditions, there are no health hazards of visible light. Visible light satisfies the eye-and-skin safety regulations [12].
- Energy efficiency: LEDs are energy efficient and highly controllable light sources, allowing them to be a part of Green technology. LEDs roughly use one twentieth of energy of a conventional light source. If all conventional light sources are replaced by LEDs, the global energy consumption would reduce by as much as 50 %, and the CO_2 emissions will also reduce [13].
- Easy implementation into existing infrastructure: VLC can be easily implemented into existing lighting infrastructure with the addition of a few relatively simple and cheap front end components [14] and [15].
- Low cost: another advantage of VLC devices is their comparably low cost. The RF links operating over approximately 10 m provide data rates of up to 1 Mb·s^{-1} in the 2.4 GHz band for a cost of nearly US $5. VLC links can transmit at 4 Mb·s^{-1} over short distances using optoelectronic devices which cost approximately US $1 [16] and [17].

LEDs have many advantages in comparison to conventional illumination sources (light bulbs and fluorescent lamps). LEDs can be switched on and off instantly. The instant on and off switching is essential for providing communication [3]. The other advantages of LEDs are higher efficiency, longer lifetime, higher tolerance to humidity, smaller and compact size, minimum heat generation compared to the conventional illumination sources, and lower power consumption. LEDs are more ecological because they are mercury free [4], [5], [18] and [19]. The key element of the VLC is a white Light Emitting Diode (LED).

LEDs provide above-described advantages, but there are also several obstructions, mainly in the communication domain. White LEDs are based on two principles [3]. The first principle uses three chips emitting blue, green and red light. If these chips are correctly power supplied, they create white light together. This principle is called colour mixing. The other principle is based on the conversion of the emitted wavelength to another wavelength. The converters are luminophores which convert blue light to yellow. The most often used luminophores are Yttrium Aluminium Garnets ($Y_3Al_5O_{12}$). The basis is the blue light emitting chip. This blue light excites the luminophore layer and a part of blue light is converted to yellow light. The rest of the blue light and the yellow light create the white light together. Both of these methods have their limitations. The three-colour LEDs are power supplied by high current, therefore, the fast on and off switching is problematic. Whereas the LEDs with the luminophore suffer the luminescence delay. After switching off of the exciting blue light, the luminophore still emits yellow light for some time, which extends the symbol duration time. This delay is called the luminescence decay [20], [21], [22], [23] and [24].

2. Solution of White LEDs Obstructions

This article proposes a solution that overcomes both above-described obstructions. The basis is a purposeful suppression of a part of the spectrum emitted by the white LED by using a suitable optical filter. The suppressed part is then replaced by spectral and intensity suitable LED. Both these LEDs then create the original white light.

The advantage is that the white LED emits continuously, it is not switched on and off. Also, the high forward current is not switched. There is even no luminophore decay. This LED is called as the illumination LED. Only the LED which replaces the suppressed part of the spectrum is switched on and off. The switched LED is a monochromatic LED which is supplied by lower forward current and creation of light is given only by features of semiconductor material. This LED is called the communication LED.

3. Measurement of Illumination Properties

We needed several components to realize the measurement. The basis was the white power LED. The forward current of this power LED was 700 mA. Further, a notch filter was placed to this white power LED. The notch filter suppressed a part of LEDs spectrum. The next used element was a suitable chosen communication LED. The communication LED had to fulfil the spectral properties for replacing the suppressed part. Before measurement of illumination properties, we looked for suitable LEDs (according to the spectrum) and we measured them. According to this, we choose the most suitable LED. Further, we solved the problem how to merge two light beams from the two LEDs in one. For this purpose, we used a beamsplitter 50:50. The disadvantage of this beamsplitter is that half of the optical power is waste. This waste is unallowable therefore a mirror was also used. Moreover, a diffuser was at the end for better mixing of LEDs beams. The final arrangement is shown in Fig. 1.

The white LED was supplied by constant forward current 700 mA. The forward current of the communication LED was gradually increased with the step of

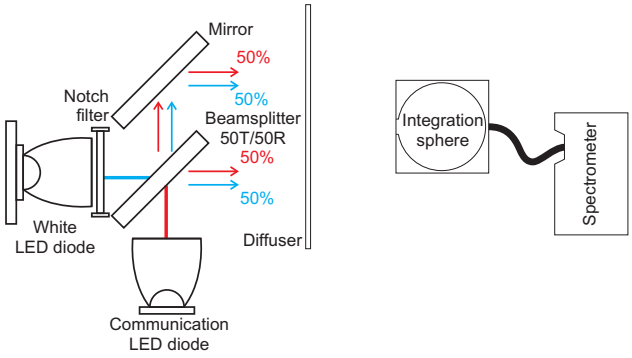

Fig. 1: Arrangement of illumination measurement.

10 mA. The aim was to find the specific forward current of the communication LED when the difference between colour coordinates x and y in CIE diagram was the smallest before and after reconstruction.

3.1. Measurement Procedure

A spectrometer with an integration sphere was used for measurement. At first, we measured the spectrum of the white power LED, Fig. 2. Furthermore, the colour coordinates and Correlated Colour Temperature (CCT) were noted. Then we put the notch filter to the white LED. The transmission of this filter is seen in Fig. 3. Thereby a part of the spectrum was suppressed. The communication LED began to emit light with the forward current 100 mA. After this setting, we measured the compound spectrum, colour coordinates x and y, and also the CCT. Then the forward current was increased with the step of 10 mA and the measurement was repeated. This procedure was done up to maximal value 350 mA of the forward current of the communication LED.

3.2. Measurement Results

The colour coordinates of original white light were $x = 0.3064$ and $y = 0.3107$, the CCT was 7070.7 K. The best reconstruction of white light came for the forward current of the communication LED 280 mA, see Fig. 4. The colour coordinates of the compound spectrum were $x = 0.3087$ and $y = 0.3108$, CCT = 6915.7 K. These measured values could be compared according to the relation, which is derived from relative error:

$$\delta(\%) = \frac{x_{rec} - x_{org}}{x_{org}} \cdot 100, \qquad (1)$$

where index *rec* means the reconstructed value and *org* is the original value. According to the Eq. (1) the colour coordinates changed less than 1 %. The CCT changed by 2.2 %. The reconstruction was very suc-

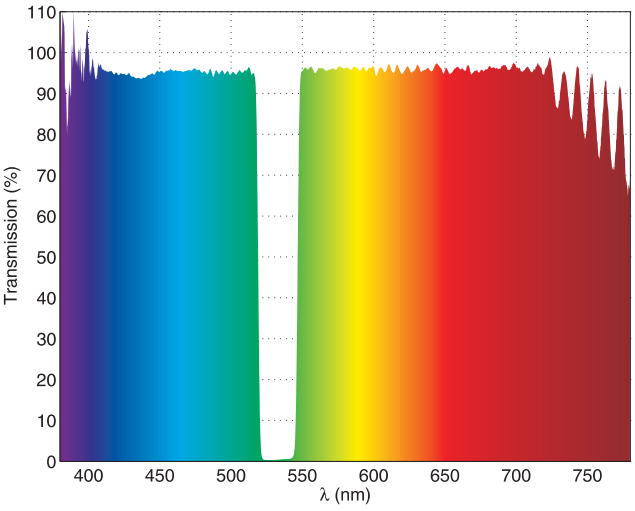

Fig. 3: Notch filter spectrum.

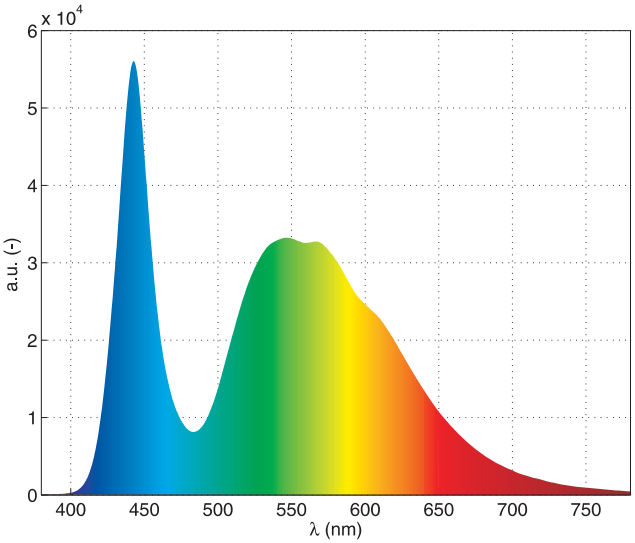

Fig. 2: White LED spectrum.

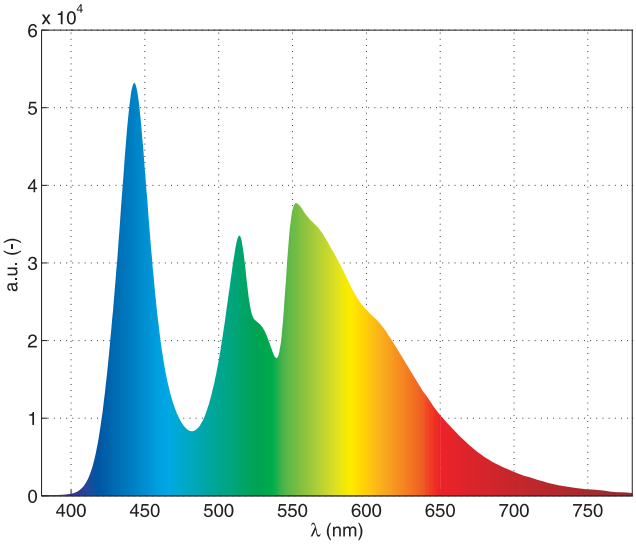

Fig. 4: Reconstructed spectrum.

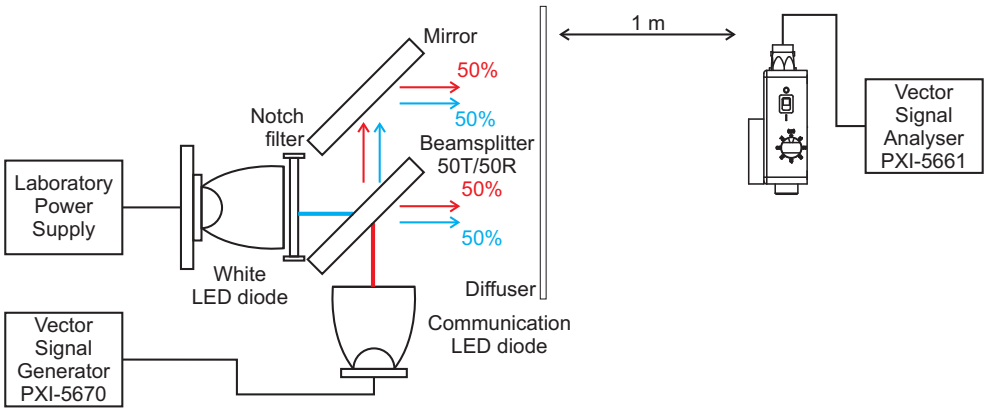

Fig. 5: Measurement of communication properties.

cessful, the measured values could be not recognized by human eye.

4. Measurement of Communication Properties

The next step was to test the communication properties of the constructed transmitter with compound spectra. The measurement was done with several pieces of equipment and instruments which are shown in Fig. 5. The Vector Signal Generator PXI-5670 created a pseudorandom sequence. This generator can create different modulation formats. A signal from PXI-5670 generator was connected to the communication LED. The illumination LED was supplied by the Laboratory Power Supply. The distance between the transmitter and the receiver was 1 m. On the receiver side, there was a PIN photodetector PDA10A-EC, its output signal was connected to the Vector Signal Analyser PXI-5661. The Analyser PXI-5661 demodulated the received signal and measured the EVM parameter. Vector Signal Generator and Analyser were connected together.

For the present, two modulation formats 4QAM and 8QAM were tested. The carrier frequencies 3 MHz and 4 MHz were set for both modulations. The changing parameter was symbol rate which was gradually increased up to communication break up. The bitrate could be calculated from the symbol rate by the help of Hartley law [25]:

$$R = f_s \cdot \log_2 M, \tag{2}$$

where R is the bitrate, f_s is the symbol rate and M is number of states, $M = 4$ for 4QAM and $M = 8$ for 8QAM. The Vector Signal Analyser PXI-5661 showed results as EVM (Error Vector Magnitude) parameter.

4.1. Error Vector Magnitude

Error Vector Magnitude (EVM) is a measurement of demodulator performance in the presence of impairments. The measured symbol location obtained after decimating the recovered waveform at the demodulator output is compared against the ideal symbol locations. The Root-Mean-Square (RMS) EVM and phase error are then used in determining the EVM measurement over a window of N demodulated symbols [26]:

$$EVM = \frac{\sqrt{\frac{1}{N}\sum_{j=1}^{N}\left[\left(I_j - \widetilde{I}_j\right)^2 + \left(Q_j - \widetilde{Q}_j\right)^2\right]}}{|\vec{v}|}, \tag{3}$$

where I_j is the I component of the j^{th} symbol received, Q_j is the Q component of the j^{th} symbol received, $\widetilde{I}_j$ is the ideal I component of the j^{th} symbol received and $\widetilde{Q}_j$ is the ideal Q component of the j^{th} symbol received, $\vec{v}$ is the ideal symbol vector. The result is expressed in percentage [26]. The EVM provides a comprehensive measure of the quality of the digitally modulated signal.

According to [27], the EVM for QAM signals is:

$$\begin{aligned} EVM_{QAM} &= \\ &= \left[\frac{1}{SNR} - 8\sqrt{\frac{3}{2\pi(M-1)SNR}}\sum_{i=1}^{\sqrt{M}-1}\gamma_i e^{\frac{3\beta_i^2 SNR}{2(M-1)}}\right. \\ &\left. + \frac{12}{M-1}\sum_{i=1}^{\sqrt{M}-1}\gamma_i\beta_i \operatorname{erfc}\left(\sqrt{\frac{3\beta_i^2 SNR}{2(M-1)}}\right)\right]^{1/2}, \end{aligned} \tag{4}$$

where $\gamma_i = 1 - \frac{i}{\sqrt{M}}$ and $\beta_i = 2i - 1$.

4.2. Measurement Results

The measured results are summarized in Fig. 6. For the end user, the most interesting is the bitrate which was calculated according to the Eq. (2). Modulation 4QAM

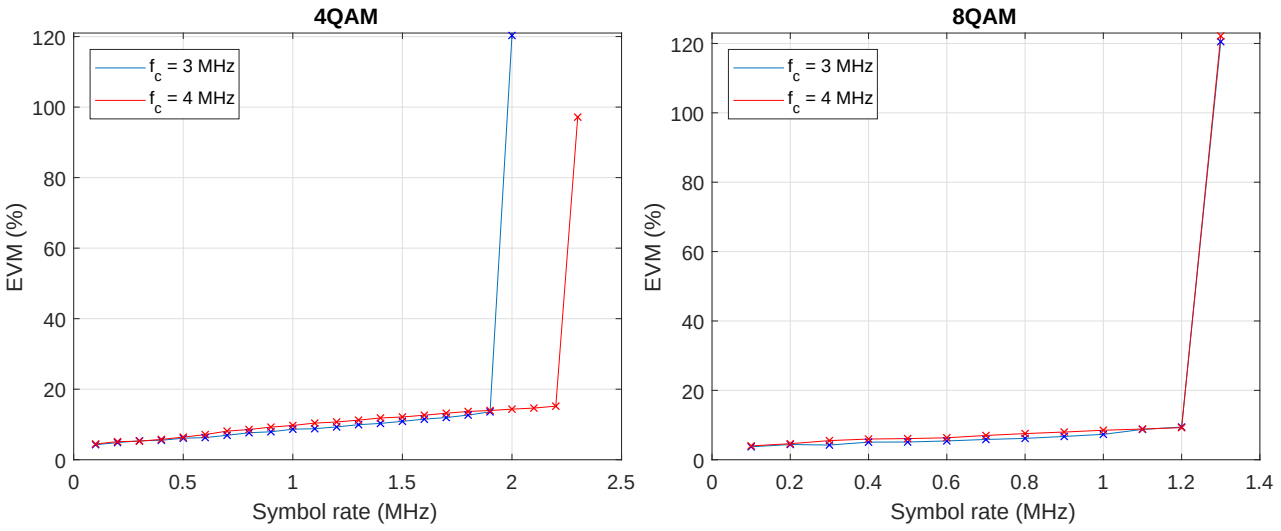

(a) 4QAM. (b) 8QAM.

Fig. 6: EVM results.

with carrier frequency $f_c = 3$ MHz reached the bitrate 3.8 Mb·s^{-1}, after that, the communication broke. Modulation 4QAM with carrier frequency $f_c = 4$ MHz reached the bitrate 4.4 Mb·s^{-1}. Modulation 8QAM with carrier frequency $f_c = 3$ MHz reached the bitrate 3.6 Mb·s^{-1}. Modulation 8QAM with carrier frequency $f_c = 4$ MHz also reached the bitrate 3.6 Mb·s^{-1} before communication break up.

5. Conclusion

This paper proposes one of the possibilities how to remove the problem with the communication properties of the white LEDs for VLC. The measured results showed that the reconstruction of the original spectrum is possible and it was very successful. The colour coordinates almost did not change, the CCT changed slightly. The differences are not recognizable by the human eye. Furthermore, the communication properties of the transmitter with suppressed and reconstructed spectrum were tested. Two modulation formats 4QAM and 8QAM were used for testing, each modulation had carrier frequencies 3 MHz and 4 MHz. The comparison of results shows that the greatest bitrate was reached with 4QAM modulation and carrier frequency 4 MHz, namely 4.4 Mb·s^{-1}. The modulation 8QAM with both carrier frequencies obtained the same results that were even worse than 4QAM modulation. The distance between the transmitter and the photodetector was only 1 m. The reason for this short distance is, above all, using the diffuser which has relative great attenuation. The solution of this problem is geometry improvement of the proposed transmitter.

Acknowledgment

The authors would like to acknowledge the financial support of the Ministry of Education, Youth and Sports of the Czech Republic under Projects No. SP2019/80 and SP2019/143 of VSB–Technical University of Ostrava, Czech Republic. Our research was also supported by Projects No. VI20172019071, VI20152020008, TA04021263, TK01020162 and TK01020178. The work has been partially supported by Project No. CZ.1.07/2.3.00/20.0217.

References

[1] CHEN, Y. C., S. S. WEN, Y. X. WU, Y. Y. REN, W. P. GUAN and Y. L. ZHOU. Long-range visible light communication system based on LED collimating lens. *Optics Communications*. 2016, vol. 377, iss. 1, pp. 83–88. ISSN 0030-4018. DOI: 10.1016/j.optcom.2016.05.036.

[2] NOVAK, T., B. SOCHA, Z. CARBOL and K. SOKANSKY. Luminance evaluation of LED indoor luminaires for workspaces lighting. In: *Proceedings of the 13th International Scientific Conference Electric Power Engineering 2012*. Ostrava: VSB–TUO, 2012, pp. 1185–1188. ISBN 978-80-214-4514-7.

[3] E. F. SCHUBERT. *Light-Emitting Diodes*. 2nd ed. Cambridge: Cambridge University Press, 2006. ISBN 978-0-521-86538-8.

[4] MINH, T. H. Q., N. H. K. NHAN, T. P. VO and N. D. Q. ANH. Enhancement of Color Rendering Index for White Light LED Lamps by Red Y_2O_3:EU^{3+} Phosphor. *Advances in Electrical and Electronic Engineering*. 2016, vol. 14, no. 3, pp. 340–344. ISSN 1804-3119. DOI: 10.15598/aeee.v14i3.1642.

[5] MARE, R. M., C. E. CUGNASCA, C. L. MARTE and G. GENTILE. Intelligent transport systems and visible light communication applications: An overview. In: *IEEE Conference on Intelligent Transportation Systems*. Rio de Janeiro: IEEE, 2016, pp. 2101–2106. ISBN 978-1-5090-1889-5. DOI: 10.1109/ITSC.2016.7795896.

[6] KARUNATILAKA, D., F. ZAFAR, V. KALAVALLY and R. PARTHIBAN. LED Based Indoor Visible Light Communications: State of the Art. *IEEE Communications Surveys & Tutorials*. 2015, vol. 17, iss. 3, pp. 1649–1678. ISSN 1553-877x. DOI: 10.1109/COMST.2015.2417576.

[7] OH, M. A flicker mitigation modulation scheme for visible light communications. In: *International Conference on Advanced Communication Technology (ICACT)*. PyeongChang: IEEE, 2013, pp. 933–936. ISBN 978-1-4673-3148-7.

[8] HOSAKO, I., N. SEKINE, M. PATRASHIN. At the Dawn of a New Era in Terahertz Technology. *Proceedings of the IEEE*. 2007, vol. 95, iss. 8, pp. 1611–1623. ISSN 0018-9219. DOI: 10.1109/JPROC.2007.898844.

[9] WOOD, R. Wireless network traffic worldwide: forecasts and analysis 2014–2019: Research Forecast Report. *Analysys Mason* [online]. 2014. Available at: `www.analysysmason.com`.

[10] KIM, S.-M. and S.-M. KIM. Performance improvement of visible light communications using optical beamforming. In: *Fifth International Conference on Ubiquitous and Future Networks (ICUFN)*. Da Nang: IEEE, 2013, pp. 362–365. ISBN 978-1-4673-5990-0. DOI: 10.1109/ICUFN.2013.6614842.

[11] MA, H., L. LAMPE a S. HRANILOVIC. Integration of indoor visible light and power line communication systems. In: *2013 IEEE 17th International Symposium on Power Line Communications and Its Applications*. Johannesburg: IEEE, 2013, pp. 291–296. ISBN 978-1-4673-6016-6. DOI: 10.1109/ISPLC.2013.6525866.

[12] WANG, Y., Y. WANG, N. CHI, J. YU and H. SHANG. Demonstration of 575-Mb/s downlink and 225-Mb/s uplink bi-directional SCM-WDM visible light communication using RGB LED and phosphor-based LED. *Optics Express*. 2013, vol. 21, iss. 1, pp. 1203–1208. ISSN 1094-4087. DOI: 10.1364/OE.21.001203.

[13] KAVEHRAD, M. Sustainable energy-efficient wireless applications using light. *IEEE Communications Magazine*. 2010, vol. 48, iss. 12, pp. 66–73. ISSN 0163-6804. DOI: 10.1109/MCOM.2010.5673074.

[14] JOVICIC, A., J. LI and T. RICHARDSON. Visible light communication: opportunities, challenges and the path to market. *IEEE Communications Magazine*. 2013, vol. 51, iss. 12, pp. 26–32. ISSN 0163-6804. DOI: 10.1109/MCOM.2013.6685754.

[15] O'BRIEN, D. C. Visible Light Communications: Challenges and potential. In: *IEEE Photonic Society 24th Annual Meeting*. Arlington: IEEE, 2011, pp. 365–366. ISBN 978-1-4244-8939-8. DOI: 10.1109/PHO.2011.6110579.

[16] RAMIREZ-INIGUEZ, R., S. M. IDRUS and Z. SUN. *Optical wireless communications: IR for wireless connectivity*. New York: CRC Press, 2007. ISBN 0-8493-7209-7.

[17] *Infrared Data Association* [online]. 2012. Available at: `http://www.irda.org/`.

[18] LINER, A., M. PAPES, J. JAROS, F. PERECAR, L. HAJEK, J. LATAL, P. KOUDELKA and V. VASINEK. Software Design of SMD LEDs for Homogeneous Distribution of Irradiation in the Model of Dark Room. *Advances in Electrical and Electronic Engineering*. 2015, vol. 12, no. 6, pp. 622–630. ISSN 1804-3119. DOI: 10.15598/aeee.v12i6.1297.

[19] STRATIL, T., P. KOUDELKA, R. MARTINEK and T. NOVAK. Active Pre-Equalizer for Broadband over Visible Light. *Advances in Electrical and Electronic Engineering*. 2017, vol. 15, no. 3, pp. 553–560. ISSN 1804-3119. DOI: 10.15598/aeee.v15i3.2210.

[20] CHEN, J., W. CRANTON and M. FIHN. *Handbook of visual display technology*. New York: Springer, 2012. ISBN 978-3-540-79566-7.

[21] WANG, Y., T. LAN and G. NI. Optical receiving system based on a compound parabolic concentrator and a hemispherical lens for visible light communication. *Applied Optics*. 2016, vol. 55, iss. 36, pp. 10229–10238. ISSN 0003-6935. DOI: 10.1364/AO.55.010229.

[22] FALL, M., G. YAN and Z. ZHONG. Visible Light Communication System Based on

Hadamard Coded 64/QAM-OFDM Signal. *International Journal of Future Generation Communication and Networking*. 2017, vol. 10, iss. 4, pp. 61–70. ISSN 2233-7857.

[23] HONG, Y., J. XU and L.-K. CHEN. Experimental investigation of multi-band OCT precoding for OFDM-based visible light communications. *Optics Express*. 2017, vol. 25, iss. 11, pp. 12908–12914. ISSN 1094-4087. DOI: 10.1364/OE.25.012908.

[24] KHALLAF, H. S., A. S. GHAZY, H. M. H. SHALABY and S. S. A. OBAYYA. Performance analysis of visible light communication systems over fading channels. In: *19th International Conference on Transparent Optical Networks (ICTON)*. Girona: IEEE, 2017, pp. 1–4. ISBN 978-1-5386-0859-3. DOI: 10.1109/ICTON.2017.8024762.

[25] HARTLEY, R. V. L. Transmission of Information. *Bell System Technical Journal*. 1928, vol. 7, iss. 3, pp. 535–563. ISSN 0005-8580. DOI: 10.1002/j.1538-7305.1928.tb01236.x.

[26] Modulation Error Ratio (MER) and Error Vector Magnitude (EVM). *National Instrument* [online]. 2014. Available at: `http://www.ni.com/white-paper/3652/en/`.

[27] MAHMOUD, H. A. and H. ARSLAN. Error vector magnitude to SNR conversion for nondata-aided receivers. *IEEE Transactions on Wireless Communications*. 2009, vol. 8, iss. 5, pp. 2694–2704. ISSN 1536-1276. DOI: 10.1109/TWC.2009.080862.

About Authors

Jan VITASEK was born in Opava, Czech Republic. In 2009 he finished M.Sc. study at Brno University of Technology, Faculty of Electrical Engineering and Communication. In 2014 he finished Ph.D. study at Department of Telecommunications, VSB–Technical University of Ostrava. His interests are Free Space Optics, indoor Free Space Optics networks and visible light communication. He is engaged in project dealing with VLC.

Jan LATAL was born in Prostejov, Czech Republic. In 2006 he was awarded his B.Sc. degree and in 2008 M.Sc. degree at VSB–Technical University of Ostrava, Faculty of Electrical Engineering and Computer Science, Department of Telecommunications in 2008. He defended his Ph.D. thesis in 2015, and he works in the field of Wireless Optical Communications, Optical Communications and Distributed Temperature Sensing Systems.

Tomas STRATIL was born in 1990 in Olomouc, Czech republic. In 2015 He received Master's degree in optical communication from VSB–Technical University of Ostrava. His research interests include Visible Light Communication and Smart technologies.

Stanislav HEJDUK was born in Ostrava, Czech Republic, in November 1985. He received his M.Sc. degree in telecommunication technologies from VSB–Technical University of Ostrava, in 2010. In 2017 he finished Ph.D. study at Department of Telecommunications, VSB–Technical University of Ostrava. His research focuses on transmitters for Mobile Free-Space Optical Communications.

Ales VANDERKA was born in 1988 in Vitkov, Czech Republic. He finished M.Sc. study at the VSB–Technical University of Ostrava, Faculty of Electrical Engineering and Computer Science, Department of Telecommunications in 2013. In present time he is Ph.D. student at VSB–Technical University of Ostrava. He focuses on optical technologies and especially Free Space Optic.

Lukas HAJEK was born in 1989 in Bohumin, Czech Republic. In 2013 he finished M.Sc. study at VSB–Technical University of Ostrava, Faculty of Electrical Engineering and Computer Science, Department of Telecommunications. In present time he is Ph.D. student at VSB–Technical University of Ostrava. His interests are Free Space Optics and aging of optical communication components.

Jakub KOLAR is currently a Ph.D. student with the Department of Telecommunications, Faculty of Electrical Engineering and Computer Science, VSB–Technical University of Ostrava.

Institute of Advanced Engineering and Science

International Journal of Electrical and Computer Engineering (IJECE)
Vol. x, No. x, May 2013, pp. 1 – 12
ISSN: 2088-8708

Measurement of Colour Coordinates of LEDs Used in the Automotive Exterior Lighting

Jan Latal[*], Patrik Hanulak[**], Jakub Kolar[*], Zdenek Wilcek[*], Tomas Stratil[*], and Filip Sarlej[*]
[*]Department of Telecommunications, Faculty of Electrical Engineering and Computer Science, VSB–Technical University of Ostrava, 17. listopadu 2172/15, 708 00 Ostrava, Czech Republic
[**]Core Optics Department, Varroc Lighting Systems, Suvorovova 195, 742 42 Senov u Noveho Jicina, Czech Republic

Article Info

Article history:
Received October 4, 2019
Revised
Accepted

Keyword:
Automotive
colour bin
colour coordinates
LED
temperature
spectral characteristic

ABSTRACT

Article deals with dichromatic white LEDs (Light-Emitting Diode) color coordinates used in automotive exterior lighting. This article also describes basic white automotive LED functionality and basic physical processes that create white light of these LEDs. It focuses on measuring color coordinates of white automotive LEDs with different temperature of LED and how the LEDs color depends on LEDs temperature. The article is comparing very important datasheet information of LED producers and values measured in the laboratory at university. The article contains statistical results of measurements and graphical representation of measured values and declared color bins which are very important for producers of headlamps for automotive companies.

Corresponding Author:
Jan Latal
Department of Telecommunications, Faculty of Electrical Engineering and Computer Science,
VSB–Technical University of Ostrava, 17. listopadu 2172/15, 708 00 Ostrava, Czech Republic
Phone: +420 597 325 845
Email: jan.latal@vsb.cz

1. INTRODUCTION

Color coordinates of LED are important when adjusting color temperature of various light sources in car head or rear lamps. New trends in automotive lighting combine various light sources as halogen bulbs, High-Intensity Discharge (HID, also known as xenon lights), and LEDs. Each of these sources has different color and each customer has different requirements on color matching of headlamp functions. Usually, color of the white light is expressed as color temperature. The temperature of an ideal black body radiator that radiates light is meant by the color temperature of a light source. For illustration, the color temperature of halogen bulbs is appx. 3500 K, the color temperature of HID is usually 4500 K and the color temperature of LED is changing from 3000 K to 6000 K, depending on producers and a LED type. Generally, bluish LEDs (from 4500 K to 6000 K) are usually chosen for car white lighting functions [1]. When more types of light sources are used in the cars headlamp, e.g. halogen bulb for high beam, HID for low beam and LED for position and Day time Running Lights (DRL) functions, the color of light sources is becoming a very important design feature. It is also possible to measure the dominant wavelength, peak wavelength, Correlated Color Temperature (CTT) or the Color Rendering Index (CRI) [2], [3], as well as spectral characteristics of the LED sources which were measured with the help of semi-empirical model based on the solid-state theory depending on the temperature. In this article, the composite author also dealt with an idea of temperature influences on colorimetric changes (chromaticity) [4]. Generally, the white LEDs for indoor illumination and similar applications are described by the parameters CCT or CRI [2]. White LEDs are usually described by chromaticity coordinates [5] which is only the way how to characterize different white light sources. Measuring and unification of white light emitted by the source is not only the task for the automotive industry. In general, it is also the task for illumination applications [6]. In the past, the temperature efficiency practical examination of the white LED Luxeon REBEL under different temperature conditions were carried out. In the past, the temperature efficiency practical examination of the white LED Luxeon REBEL under different temperature conditions were carried out [7]. Measuring LEDs characteristics

using the integration sphere has been carried out by many researchers, which is one of the most reliable ways how to measure LEDs [1], [8] and [9]. Various researches about measuring LED junction temperature were also made. One of the ways how to control LED temperature is by measuring the forward voltage of LED which was in the oil bath of specific temperature [8]. It has been proved that output luminous flux substantially changes with the temperature by implementation of the LED into the integration sphere and brings in fatal errors in determining the LED properties [10]. Measuring the temperature of the LED transition with the help of various experiments was reached by contact and contactless measurement [11]. Measurement of optical and electrical properties and calculation of the transition temperature was attained in the publication [12]. Another approach is mathematical–LED junction temperature can be calculated from its forward voltage [9]. This solution is very accurate, but it is limited by accuracy of measurement equipment. Modelling of temperature changes of LED diodes by Computational Fluid Dynamics (CFD) analysis was also discussed in the article [13], [14] and [15]. The Fan et. all focused on degradation of LED aging and changes in spectral power distribution and efficiency. The LED chip parameters and its aging over time, as well as temperature, phosphorus and polymer used for the LED were measured. The process of the shift of LED elements, which is not linear, was monitored, and non-linear state-space model was developed. It predicts the time of CSF failure (Color Shift Failure) [16]. The physical properties of the LEDs in time were also tested. It was monitored how their parameters would change, e. g. illumination, current through the LED on operation time, efficiency coefficient on operation time, etc. [17]. A team of authors Qu focused on the LED temperature measurement and aging of installations while using Pulse Width Modulation (PWM) for the RGB (Red, Green, Blue) LED. It has been found out that the PWM modulation technique can effectively control color/luminosity without the necessity of feedback [18]. Similar results were achieved by another team of Umar and others [19] who designed a DC-DC converter with PWM lighting control or Dyble [20] and Gu [21]. Other way how to measure LED temperature is by using a sensor which contacts with Printed Circuit Boards (PCB) near LED solder point [22], [23].

The measurements in this article aimed to find a process of measuring the color coordinates of white LEDs in the real applications in the company Varroc Lighting System without using any special laboratory equipment. This process should be very simple easy enough for repeating even by a person that has only basic optical and electrical knowledge. For this reason, measuring of the color coordinate by integrating sphere and spectrometer and measuring the temperature of LED by the thermal camera was chosen and recommended to the company Varroc Lighting Systems. Based on the measured data, conclusions and recommendations on how to work with different types of LED batches from different suppliers are made to minimize changes in the light emitted and negative impact on production.

2. AUTOMOTIVE WHITE LED

In the automotive industry, is usually used only one type of white LED – blue LED with luminophore that is converting blue light into white. In that case a luminophore, yttrium-aluminum garnet activated by cerium is usually used. This material is activated by blue light of the InGaN diode. In automotive industry, usually only one type of white LED is used blue LED with luminophore. The luminophore is Yttrium-Aluminium Garnet (YAG) doped by cerium in most cases. The YAG is activated by blue light from InGaN diode and it converts a part of blue light in yellow light. This yellow light is mixed together with the rest of blue light. Correct proportions of lights (blue and yellow) create white light. LED producers divide each type of LED into various groups according to the color coordinates in CIE *x, y* chromaticity diagram. These groups are called color bins. Differences in LED color and dividing LED into various bins is caused by technology of LED production. For LED production, a simple substrate is used. On the surface of the substrate thin crystalloid layer is grown. This process is called epitaxy. As a result, semiconductor forming die of blue LED is created. This semiconductor is cut to small pieces afterwards. The electrical connections are inserted and layer or suspension of luminophore is added into its surrounding. This setup is encapsulated and creates a white LED. The luminophore layer is thin in order 10^{-2} mm, epitaxy processes create natural differences in LED properties [8]. Even the manufacturers are trying to minimize these differences; it is not possible to create highly consistent and strictly controlled LED production with the same characteristics. For this reason, LEDs are divided into groups with similar characteristics. These groups are called bins and they can be organized into three main groups: by luminous flux, color coordinates and voltage.

2.1. Sorting Automotive LEDs According to Colour Coordinates

Manufacturers sort LEDs to color bins according to their x and y coordinates in chromaticity diagram defined in CIE 1931. These bins are defined usually by 4 points that create convex rectangle in chromaticity diagram. Pentagons or hexagons defining color bin are not unusual, too. Size of the bins depends on manufacturing quality generally, the more accurate production, the smaller color bins can be produced.

Table 1. List of measured LEDs.

LED type	Bin	Nominal current [mA]	Light temperature
Seoul SZW05A0A Z5	U2C3H	350	Cool
Seoul SZW05A0A Z5	U2E7I	350	Neutral
Seoul SZW05A0A Z5	U3C8I	350	Cool
Seoul SZW05A0A Z5	U1D5H	350	Neutral
Seoul SPW08F0D P8	-	350	Cool
Osram OSTAR LE UW D1W4 01	JM	700	Cool
Luxeon Rebel LXML PWN1 0100	NTPD	350	Neutral

3. EXPERIMENT REQUIREMENTS AND DESCRIPTION

The task of the measurement was to measure color coordinates of white automotive LEDs in the range of different temperature of LED and to evaluate the difference between color coordinates of LEDs in different temperatures. All measurements were aimed at automotive industry needs, so measuring of color coordinates was chosen for this purpose. A dark room was used to prevent direct light to affect the results of experiments. Measurements were made in a special dark room situated in VSB–Technical University of Ostrava. Sizes of the dark room were $2.6 \times 3 \times 2.5$ m. Amount of photons in this room was only 7 photons per second (Declared dark counts of photodetector 1 cps). Setup scheme consists of LED, Peltier cooler, CPU cooler and fan as it is shown in Fig. 1.

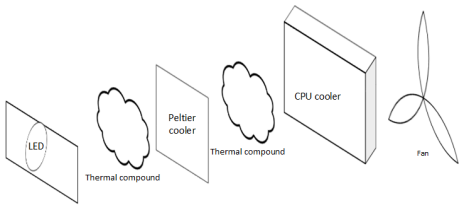

Figure 1. LED thermal regulation system assembly.

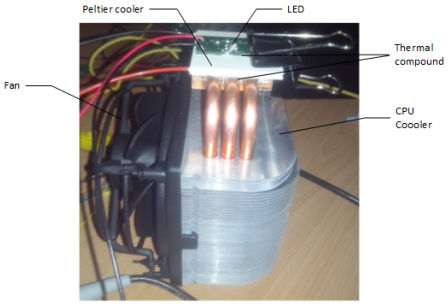

Figure 2. Thermal control system for measurements.

The real final setup can be seen in Fig. 2. All main components are described in the paragraph above. All experimental measurements were made $30\times$ for each LED and each temperature. The types of LEDs used for measurements can be found in Tab. 2. All LEDs are certified for using in the automotive industry and are proven as light sources for the automotive industry. Seoul LEDs are a simple and cheap example of automotive LED; they are widely used owing to their low price and a good luminous flux. Luxeon Rebel LEDs are known because of their great thermal management and thermal stability. Osram OSTAR LED used in this experiment is powerful 4-chip LED with a very high luminous output. Aim of the measurement was to verify the hypothesis that the colour coordinates change with the growing temperature of LED. As the P-N junction is situated inside of the LED structure, temperature of the LEDs surface T_s was measured.

4. MEASUREMENT RESULTS

LEDs were measured for various temperatures of surface and the nominal current of LEDs was kept. Color coordinates were measured by the following procedure:

- Assembly of the thermal control system (Fig. 1 and Fig. 2).

- Connecting electronic components (Peltier cooler, fan, LED) to power supplies.
- Setting the nominal current of LED according to producers datasheet.
- Turning on power supplies for Peltier cooler and fan.
- Monitoring LEDs surface using thermocamera, regulation of temperature using Peltier cooler and LEDs forward current until the temperature on LEDs surface and forward current reach the values defined in vendors datasheet.
- Measuring color coordinates using Avantes spectrometer and integration sphere.
- Changing LEDs surface temperature by adjusting Peltier cooler current.
- Adjusting LEDs forward current to nominal.

All results were placed into the graph with proper bin definitions and bins tolerances. Osram OSTAR LE UW D1W4 01 nominal temperature was not measured according to the datasheet, because the vendor provides information about color shift according to temperature changes and the LED was already assembled on its cooler. This does not allow fitting it on the cooling system described in Fig. 4. Results for each LED were compared for nominal temperature and heated LED. All results were evaluated using exploratory statistic methods of data analysis and the following statistical data were calculated: Mean (μ), Median ($\widetilde{x}$), Mode ($\widehat{x}$), 75 % quartile, 25 % quartile ($Q_{0.75}$ $Q_{0.25}$), Minimum, maximum and Variance (σ_2). All measured values of color coordinates were tested for mean equation based on the test of the significance difference of the two sample averages (t-test). Hypotheses were tested for 95 % confidence interval separately for x and y coordinates. The following chapters gradually describe the results of experimental measurements and then the processing by means of the Statgraphics Centurion XV. The different types of LED boards with LEDs were always labelled according to the bin to which the LED type fell. As can be seen in Fig. 2, a zero series resistor was used for all the LED samples, and therefore, it was not necessary to perform exhaustive calculations to determine the electric current flowing through the tested LEDs.

4.1. Seoul Semiconductors Z5

First of the tested LED was Seoul Semiconductors (SSC) Z5 LED shown in Fig. 3.

Figure 3. LED seoul semiconductors Z5 assembled.

Following Fig. 4 shows distribution of heat on PCB and areas on PCB used for the thermal management measurements by thermocamera for 25 °C, or for 93.9 °C on the LED sample SSC Z5 LED. The thermocamera was aimed at the LED. As can be seen on the left part of the picture, these areas have higher temperature as they are leading a heat away. On the right part of the picture there is the cooler that cant handle all the heat.

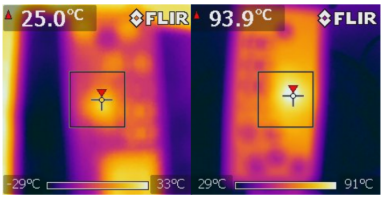

Figure 4. Heat distribution on PCB assembled with SSC Z5 LED.

4.1.1. U2C3H

Statistical results for LED SSC Z5 binned as U2C3H are shown in Tab. 2. After, we found the basic statistical functions and outputs it was proceeded to more thorough analysis based on hypotheses through t-test.

Table 2. Results of SSC Z5 U2C3H.

Surface temperature	$\mathbf{T_s = 25\ °C}$		$\mathbf{T_s = 100\ °C}$		Difference	
Coordinates	**x**	**y**	**x**	**y**	**x**	**y**
Mean	0.3643	0.3755	0.3659	0.3827	0.0016	0.0072
Median	0.364	0.375	0.366	0.383	0.002	0.007
Modus	0.364	0.375	0.366	0.383	0.002	0.007
75 % quartile	0.365	0.376	0.36675	0.383	0.002	0.008
25 % quartile	0.364	0.375	0.365	0.382	0.001	0.00625
Minimum	0.364	0.375	0.363	0.381	−0.002	0.005
Maximum	0.365	0.377	0.368	0.386	0.004	0.011
Variance	0.0004661	0.0005724	0.001094	0.0013429	0.0012484	0.0016692

Table 3. Results of SSC Z5 U2E7I.

Surface temperature	$\mathbf{T_s = 25\ °C}$		$\mathbf{T_s = 100\ °C}$		Difference	
Coordinates	**x**	**y**	**x**	**y**	**x**	**y**
Mean	0.3915	0.3689	0.4052	0.389	0.0137	0.0192
Median	0.391	0.37	0.405	0.389	0.014	0.019
Modus	0.391	0.37	0.406	0.389	0.014	0.018
75 % quartile	0.392	0.37075	0.406	0.39	0.014	0.02075
25 % quartile	0.391	0.369	0.40425	0.38725	0.013	0.018
Minimum	0.388	0.368	0.402	0.385	0.009	0.015
Maximum	0.393	0.371	0.408	0.392	0.017	0.024
Variance	0.0010417	0.0009248	0.0012847	0.0018473	0.0016174	0.0021669

Hypothesis test for x–coordinates:

$$\begin{aligned} H_0 &: \mu(x)_{T_s=25} = \mu(x)_{T_s=100}, \\ H_A &: \mu(x)_{T_s=25} \neq \mu(x)_{T_s=100}, \end{aligned} \tag{1}$$

Hypothesis test shows that temperature change has influenced color coordinates x and y for LED SSC Z5 U2C3H. Comparison of measured results for T_s with data declared by the vendor is shown in Fig. 5.

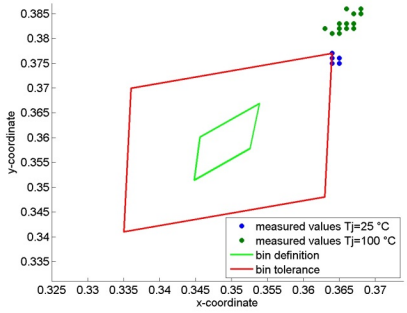

Figure 5. Comparison of measured values to companys information for SSC Z5 LED binned as U2C3H.

4.1.2. U2E7I

Statistical results for LED SSC Z5 binned as U2E7I are in Tab. 3, where we can observe that the changes range at very low levels.

Hypothesis test for x–coordinates:

$$\begin{aligned} H_0 &: \mu(x)_{T_s=25} = \mu(x)_{T_s=100}, \\ H_A &: \mu(x)_{T_s=25} \neq \mu(x)_{T_s=100}, \end{aligned} \tag{2}$$

$P - Value = 0 \ll 0.05 \longrightarrow$ rejecting H_0 on confidence interval 95 %.

Hypothesis test for y–coordinates:

$$\begin{aligned} H_0 &: \mu(y)_{T_s=25} = \mu(y)_{T_s=100}, \\ H_A &: \mu(y)_{T_s=25} \neq \mu(y)_{T_s=100}, \end{aligned} \tag{3}$$

Table 4. Results of SSC Z5 U3C8I.

Surface temperature	$\mathbf{T_s = 25\ °C}$		$\mathbf{T_s = 100\ °C}$		Difference	
Coordinates	x	y	x	y	x	y
Mean	0.3517	0.376	0.355	0.3839	0.0033	0.0079
Median	0.352	0.376	0.354	0.385	0.003	0.009
Modus	0.352	0.376	0.354	0.385	0.002	0.009
75 % quartile	0.352	0.376	0.357	0.385	0.005	0.009
25 % quartile	0.351	0.375	0.353	0.384	0.00125	0.008
Minimum	0.35	0.373	0.352	0.358	−0.002	−0.018
Maximum	0.355	0.379	0.36	0.388	0.009	0.012
Variance	0.0011492	0.0013391	0.0023413	0.005047	0.0028032	0.0050265

Table 5. Results of SSC Z5 U1D5H.

Surface temperature	$\mathbf{T_s = 25\ °C}$		$\mathbf{T_s = 100\ °C}$		Difference	
Coordinates	x	y	x	y	x	y
Mean	0.3754	0.3671	0.3837	0,375	0.0083	0.0079
Median	0.375	0.367	0.385	0,376	0.0095	0.009
Modus	0.375	0.368	0.385	0,376	0.01	0.009
75 % quartile	0.376	0.368	0.385	0,377	0.01	0.01
25 % quartile	0.375	0.366	0.384	0,375	0.009	0.008
Minimum	0.375	0.366	0.355	0,36	−0.02	−0.006
Maximum	0.376	0.368	0.386	0,378	0.011	0.012
Variance	0.0005040	0.0008996	0.0055207	0,0041021	0.0054719	0.0040406

$P - Value = 0 \ll 0.05 \longrightarrow$ rejecting H_0 on confidence interval 95 %. Hypothesis test shows that temperature change has influenced color coordinates x and y for LED SSC Z5 U2E7I. Comparison of measured results of T_s with data declared by vendor is shown in the following Fig. 6.

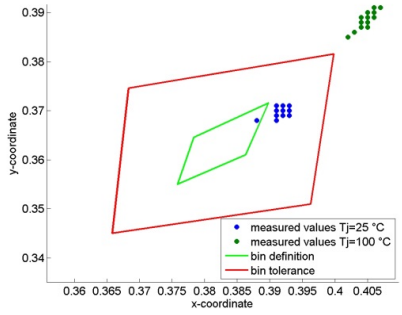

Figure 6. Comparison of measured values to companys information for SSC Z5 LED binned as U2E7I.

4.1.3. U3C8I

The basic statistical analyses were again used according to the exploratory analysis through the Statgraphics Centurion XV software environment for the LED SSC Z5 binned as U3C8I. Statistical results for LED are shown in Tab. 4. Afterwards, the analysis through the t-test based on the hypotheses was proceeded to find out whether the mean values differ at a significant level.

Hypothesis test for x–coordinates:

$$\begin{aligned} H_0 &: \mu(x)_{T_s=25} = \mu(x)_{T_s=100}, \\ H_A &: \mu(x)_{T_s=25} \neq \mu(x)_{T_s=100}, \end{aligned} \tag{4}$$

$P - Value = 5.03093 \cdot 10^{-9} \ll 0.05 \longrightarrow$ rejecting H_0 on confidence interval 95 %.

Hypothesis test for y–coordinates:

$$\begin{aligned} H_0 &: \mu(y)_{T_s=25} = \mu(y)_{T_s=100}, \\ H_A &: \mu(y)_{T_s=25} \neq \mu(y)_{T_s=100}, \end{aligned} \tag{5}$$

$P - Value = 2.02931 \cdot 10^{-11} \ll 0.05 \longrightarrow$ rejecting H_0 on confidence interval 95 %

Hypothesis test shows that the temperature change has influenced color coordinates *x* and *y* for LED SSC Z5 U3C8I. Comparison of measured results of T_s with data declared by vendor is shown in the following Fig. 7.

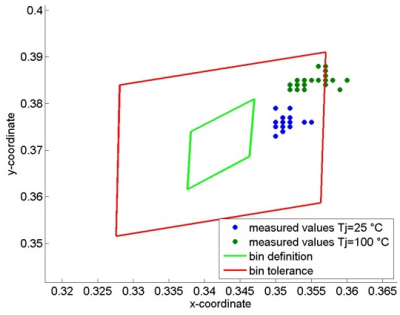

Figure 7. Comparison of measured values to companys information for SSC Z5 LED binned as U3C8I.

4.1.4. U1D5H

Statistical results for LED SSC Z5 binned as U1D5H are shown in Tab. 5.

Hypothesis test for x–coordinates:

$$\begin{aligned} H_0 &: \mu(x)_{T_s=25} = \mu(x)_{T_s=100}, \\ H_A &: \mu(x)_{T_s=25} \neq \mu(x)_{T_s=100}, \end{aligned} \tag{6}$$

$P - Value = 2.82712 \cdot 10^{-11} \ll 0.05 \longrightarrow$ rejecting H_0 on confidence interval 95 %.

Hypothesis test for y–coordinates:

$$\begin{aligned} H_0 &: \mu(y)_{T_s=25} = \mu(y)_{T_s=100}, \\ H_A &: \mu(y)_{T_s=25} \neq \mu(y)_{T_s=100}, \end{aligned} \tag{7}$$

$P - Value = 0 \ll 0.05 \longrightarrow$ rejecting H_0 on confidence interval 95 %. Hypothesis test shows that temperature change has influenced color coordinates *x* and *y* for LED SSC Z5 U1D5H. Comparison of measured results of T_s with data declared by vendor is shown in the following Fig. 8.

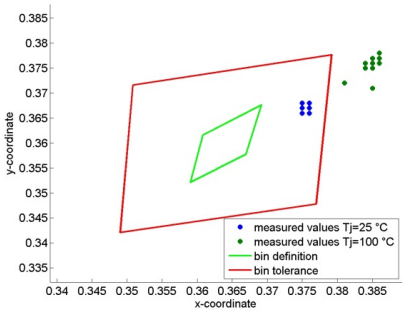

Figure 8. Comparison of measured values to companys information for SSC Z5 LED binned as U1D5H.

4.2. Seoul Semiconductors P8

For SSC P8 LED measurement, the same procedure was used as for SSC Z5. As this LED was only for demonstrational purposes, it was not binned in any color bin. Nominal current for this LED is 350 mA, lower temperature limit 25 °C, the highest measured temperature was 100 °C. Photo of SSC P8 can be seen in Fig. 9, heat distribution on PCB is shown in Fig. 10.

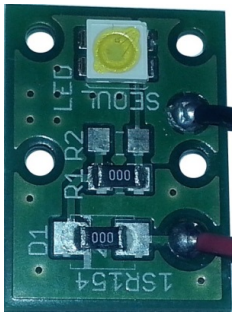

Figure 9. LED seoul semiconductors P8 assembled on PCB.

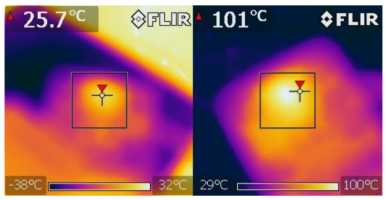

Figure 10. Heat distribution on PCB assembled with SSC P8 LED.

PCB for this LED has little bit worse ability for heat leading. This is the reason why the holes for heat leading not clearly visible on thermocamera pictures. Statistical results for LED SSC P8 are shown in Tab. 6.

Hypothesis test for x–coordinates:

$$\begin{aligned} H_0 &: \mu(x)_{T_s=25} = \mu(x)_{T_s=100}, \\ H_A &: \mu(x)_{T_s=25} \neq \mu(x)_{T_s=100}, \end{aligned} \tag{8}$$

$P - Value = 0 \ll 0.05 \longrightarrow$ rejecting H_0 on confidence interval 95 %.

Hypothesis test for y–coordinates:

$$\begin{aligned} H_0 &: \mu(y)_{T_s=25} = \mu(y)_{T_s=100}, \\ H_A &: \mu(y)_{T_s=25} \neq \mu(y)_{T_s=100}, \end{aligned} \tag{9}$$

$P - Value = 0 \ll 0.05 \longrightarrow$ rejecting H_0 on confidence interval 95 %. Hypothesis test shows that temperature change has influenced color coordinates *x* and *y* for LED SSC P8. Comparison of measured results of different T_s is shown in the following Fig. **??**.

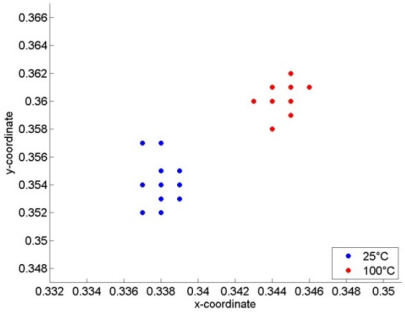

Figure 11. Comparison of colour coordinates between different temperatures of LED SSC P8.

4.3. Philips Luxeon Rebel PWN1 0100 NTPD

Vendor Philips has other criteria for color coordinates measuring temperature. They recommend measuring the temperature of the LED using pad situated on the PCB near LED solder point known as T_{pad}. For this measurement, the same technology of measuring LED temperature is used for all other LEDs. Generally, the equation

Table 6. Results for LED SSC P8.

Surface temperature	$T_s = 25\ °C$		$T_s = 100\ °C$		Difference	
Coordinates	x	y	x	y	x	y
Mean	0.3381	0.3537	0.3445	0.3606	0.0064	0.0069
Median	0.338	0.354	0.345	0.361	0.006	0.007
Modus	0.338	0.354	0.345	0.361	0.006	0.007
75 % quartile	0.339	0.354	0.345	0.361	0.007	0.008
25 % quartile	0.338	0.353	0.344	0.36	0.006	0.00625
Minimum	0.337	0.352	0.343	0.358	0.005	0.003
Maximum	0.339	0.357	0.346	0.362	0.008	0.01
Variance	0.0006815	0.0012848	0.0006789	0.0008137	0.0009714	0.0015698

Table 7. Results of Philips Luxeon Rebel NTPD LED.

Surface temperature	$T_s = 25\ °C$		$T_s = 100\ °C$		Difference	
Coordinates	x	y	x	y	x	y
Mean	0.3767	0.3697	0.3822	0.3814	0.0055	0.0117
Median	0.376	0.3695	0.382	0.382	0.0055	0.0125
Modus	0.376	0.369	0.382	0.382	0.005	0.013
75 % quartile	0.377	0.37	0.383	0.383	0.006	0.013
25 % quartile	0.376	0.369	0.382	0.38125	0.005	0.011
Minimum	0.376	0.369	0.379	0.363	0.003	−0.007
Maximum	0.379	0.372	0.387	0.387	0.009	0.017
Variance	0.0009154	0.0008684	0.0012972	0.003748	0.0013582	0.0039034

$T_{pad} = T_s - 17.64$ can be used for conversion between T_{pad} and T_s. Vendor determines inaccuracy in bin definitions 0.005 for both coordinates. PCB has a system of holes used for great thermal management, as can be seen in the following Fig. 12.

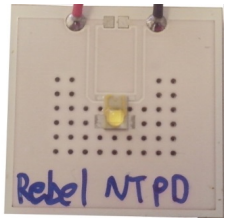

Figure 12. LED luxeon rebel assembled on PCB.

As can be seen in Fig. 13, has much better thermal management than previous LEDs. Heat is distributed evenly all over PCB. Statistical results for LED Luxeon Rebel NTPD are shown in Tab. 7.

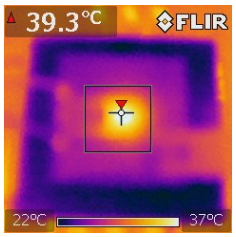

Figure 13. Heat distribution on PCB assembled with Luxeon Rebel LED.

Hypothesis test for x–coordinates:

$$\begin{aligned} H_0 &: \mu(x)_{T_s=25} = \mu(x)_{T_s=100}, \\ H_A &: \mu(x)_{T_s=25} \neq \mu(x)_{T_s=100}, \end{aligned} \tag{10}$$

$P - Value = 0 \ll 0.05 \longrightarrow$ rejecting H_0 on confidence interval 95 %.

Hypothesis test for y–coordinates:

$$H_0 : \mu(y)_{T_s=25} = \mu(y)_{T_s=100}, \\ H_A : \mu(y)_{T_s=25} \neq \mu(y)_{T_s=100}, \tag{11}$$

$P - Value = 0 \ll 0.05 \longrightarrow$ rejecting H_0 on confidence interval 95 %. Hypothesis test shows that temperature change has influenced color coordinates *x* and *y* for LED Luxeon Rebel NTPD. Comparison of measured results of T_s with data declared by vendor is shown in the following Fig. 14.

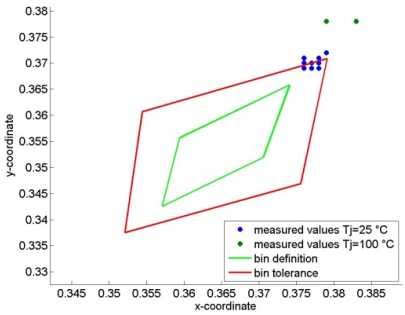

Figure 14. Comparison of measured values to companys information for LED Philips Luxeon Rebel binned as NTPD.

4.4. OSRAM LE UW D1W4 01 JM

This LED is built from 4 dies assembled on one chip. This solution offers high luminous flux (630 lm in this case) and wide area of application thanks to its small dimensions. Nominal voltage of this LED is 14.1 V, the nominal current 700 mA. PCB with LED was mounted on aluminum cooler (Fig. 15) that provides its cooling as this LED produces a lot of heat.

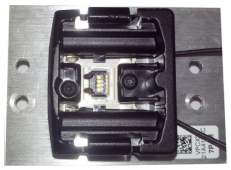

Figure 15. Heat distribution on PCB assembled with 4-chip LED Osram LE UW D1W4.

However, the temperature on the surface of LED has reached 120 °C, as shown in Fig. 16. Once the LED reaches this value, the temperature of LED is stabilized and no significant swings of temperature can be observed. As this LED was assembled on the heatsink, it was not possible to add the Peltier cooler. Vendor provides information about color coordinates shift in LEDs datasheet. Value for color shift for 120 °C and nominal current 700 mA is 0.012 for *x*–coordinate and 0.014 for **y**–coordinate. Vendor guarantees tolerance of color coordinates binning equal to 0,005. For verifying LEDs binning, color bin definitions were shifted according to information about color shifting in datasheet. Comparison of measured values and shifted vendors definitions can be seen in Fig. 17.

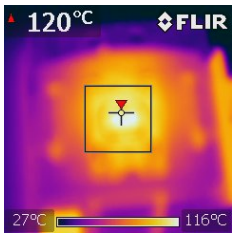

Figure 16. Thermal distribution of Osram LE UW D1W4.

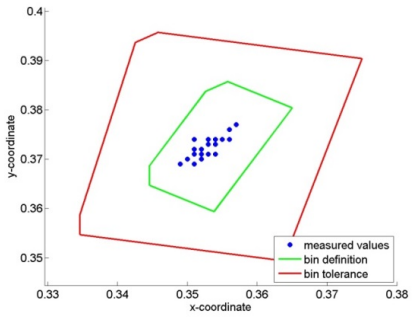

Figure 17. Comparison of measured colour coordinates and shifted bin definition for LED Osram LE UW D1W4 binned as 01JM.

5. RESULTS OF EXPERIMENT AND DISCUSSIONS

All experimental measurements proved that color coordinates of LEDs are changing according to the LED temperature. Average shift in coordinates is 0.011 for *x*–coordinate and 0.018 for *y*–coordinate. In these numbers, results of measuring two prototype LEDs have been counted unfortunately, concrete results of these two prototype LEDs cannot be published as they are still in process of development. According to the hypotheses test that rejects equality of means of measured color coordinates we can claim that there is a shift of color coordinates caused by the change of LEDs temperature. This shift is caused by change of the intensity of LED die. As mentioned before, the spectrum of white LED used for automotive industry is created by blue part of LED die and yellow/orange luminophore layer providing color conversion. LED dies luminous output is getting lower with rising temperature, but luminophore layers optical properties do not change dramatically with temperature change. This leads to a fact that less amount of blue light is converted by the same amount of luminophore layer. This means the color coordinates shift to the yellow part of chromaticity diagram. Results of this experiment can be used in automotive lighting industry for matching colors of various types of light sources as the temperature of LED changes during car operation time.

6. CONCLUSION

The measurements of different characteristics and their dependence on the temperature of the P-N transition for the most commonly used types of LED samples in the automotive industry, or more precisely for manufactures of lighting components, were made within the experimental measurements. The first hypothesis through the t-test was that the change of the temperature of the P-N transition had an effect on the shift of color coordinates. This hypothesis was confirmed after processing the measured data with statistical methods. At the same time, it has been proved that the manufacturer Seoul designates incorrectly the temperature, at which the color bins are defined, as the ambient temperature. It has been shown that the temperature control of the P-N transition is more important than the ambient temperature control in terms of achieving values given in the data sheet. The verification also determined the average value of the color coordinate shift at the temperature change of the P-N transition for the selected LED samples. The color coordinates of the specified LEDs correspond to the bin definitions given by the manufacturers and into which they were classified. In the future it will be necessary to make further measurements of other LED bathes, as the latest trends in the development and use of lighting or automotive components are driven by the demand for high-quality radiation sources that enable to reduce energy consumption and, therefore, to achieve greener operation combined with further possible use of these radiation sources, e.g. for communication via VLC.

ACKNOWLEDGEMENT

The research described in this article could be carried out thanks to the active support of the projects no. SP2019/80 and SP2019/143, VI20172019071 and CZ.1.07/2.3.00/20.0217, CZ.02.1.01/0.0/0.0/16_019/0000867.

REFERENCES

[1] Y. Ohno, et al.,Optical metrology for LEDs and solid state lighting, in *Proceedings of SPIE, Fifth Symposium Optics in Industry (6046)*, 2006, pp. 4625–4625.
[2] S. Chhajed, et al.,Influence of junction temperature on chromaticity and color-rendering properties of trichromatic white-light sources based on light-emitting diodes, *Journal of Applied Physics*, vol. 97, pp. 054506-1–054506-8,

2005.
[3] S. Chhajed, et al., Junction temperature in light-emitting diodes assessed by different methods, in *Proceedings of SPIE, Light-Emitting Diodes: Research, Manufacturing, and Applications IX (5739)*, 2005, pp. 16–24.
[4] A. Garcia-Botella, et al., Thermal influences on optical properties of light-emitting diodes: a semiempirical model, *Applied Optics*, vol. 40, pp. 533–537, 2001.
[5] T. Nagele, White Light LEDs - Importance of Accepted Measurements Standards, *LED Professional Review*, 2008, vol. Nov/Dec 2008, pp. 22–25.
[6] Philips Lumileds. [Online] Avaible from: http://www.philipslumileds.com.
[7] A. Andonova, et al., Estimation the Amount of Heat Generated by LEDs under Different Operating Conditions, *Elektronika ir Elektrotechnika*, vol. 22, pp. 49–53, April 2016.
[8] Z. Balas, et al., Kolorimetricke parametre LED pasov, Bratislava: Slovenska technicka univerzita v Bratislave, 2011.
[9] D. Peng and K. Jin, The influence of driving current on emission spectra of GaN-based LED, in *Proceedings of 2011 International Conference on Electronics and Optoelectronics*, 2011, pp. V2-148–V2-151.
[10] Y. Lei, et al., Research on the thermal property of powerful white LEDs, *Journal of Optoelectronics Laser*, vol. 17, pp. 945–947, 2006.
[11] A. Andonova, et al., Application of IRT NDT for ensuring heat robustness of LED Modules, in *Proc. 29th Intl. Conf. Microel. (MIEL 2014)*, 2014, pp. 303–306.
[12] A. Andonova, et al., Accelerated aging for LEDs, *Annual Journal of Electronics*, vol. 2, pp. 5558, 2012.
[13] A. Andonova, LED PCB thermal simulation using FLOEFD, *Eastern-European Journal of Enterprize Technologies*, vol. 6, pp. 59–61, 2012.
[14] J. Jakovenko, et al., High Power Solid State Retrofit Lamp Thermal Characterization and Modeling, *Radioengineering*, vol. 21, pp. 225–230, 2012.
[15] J. Formanek and J. Jakovenko, Thermal Characterization and Lifetime Prediction of LED Boards for SSL Lamp, *Radioengineering*, vol. 22, pp. 245–250, 2013.
[16] J. Fan, et al., Color Shift Failure Prediction for Phosphor-Converted White LEDs by Modeling Features of Spectral Power Distribution with a Nonlinear Filter Approach, *Materials*, vol. 10, pp. 1–16, 2017.
[17] V. Dumbrava, et al., Initial Investigation into the Energy and Operational Parameters of LED Modules, *Elektronika ir Elektrotechnika*, vol. 22, pp. 33–36, June 2016.
[18] X. Qu, et al., Color Control System for RGB LED Light Sources Using Junction Temperature Measurement, in *The 33rd Annual Conference of the IEEE Industrial Electronics Society (IECON)*, 2007, pp. 1363–1368.
[19] M. Wa. Umar, et al., PWM Dimming Control for High Brightness LED Based Automotive Lighting Applications, *International Journal of Electrical and Computer Engineering (IJECE)*, vol. 7, pp. 2434–2440, October 2017.
[20] M. Dyble, et al., Impact of dimming white LEDs: chromaticity shifts due to different dimming methods, in *Proceedings of SPIE, Fifth International Conference on Solid State Lighting (5941)*, 2005, pp. 291–299.
[21] Y. Gu, et al., Spectral and Luminous Efficacy Change of High-power LEDs Under Different Dimming Methods, in *Proceedings of SPIE, Sixth International Conference on Solid State Lighting (6337)*, 2006, pp. 63370J-1–63370J-7.
[22] P. Karha, et al., Radiometric Determination of the Junction Temperature of Light-emitting Diodes, in *2013, Proceedings of CIE Centenary Conference "Towards a New Century of Light*, 2013, pp. 308–316.
[23] A. Vaskuri, et al., Relationships between junction temperature, electroluminescence spectrum and ageing of light-emitting diodes, *Metrologia*, vol. 55, pp. S86–S95, 2018.